









RESEARCH ARTICLE

IGF1R expression by adult oligodendrocytes is not required in the steady-state but supports neuroinflammation

Giuseppe Locatelli^{1,2}  | Filipa Marques-Ferreira³ | Antonis Katsoulas³  |
 Vasileia Kalaitzaki³  | Martin Krueger⁴ | Barbara Ingold-Heppner⁵ |
 Sabrina Walthert² | Roman Sankowski⁶  | Olivia Prazeres da Costa⁷ |
 Amalia Dolga^{8,9} | Magdalena Huber¹⁰  | Maike Gold¹¹ | Carsten Culmsee⁸  |
 Ari Waisman¹²  | Ingo Bechmann⁴  | Vladislava Milchevskaya^{13,14}  |
 Marco Prinz^{6,15,16}  | Achim Tresch^{13,14}  | Burkhard Becher¹  | Thorsten Buch^{1,3,7} 

¹Institute of Experimental Immunology, University of Zurich, Zurich²Theodor Kocher Institute, University Bern, Bern, Switzerland³Institute of Laboratory Animal Science, University of Zurich, Zurich⁴Institute of Anatomy, University of Leipzig, Leipzig, Germany⁵Institute of Pathology, Campus Mitte, Charité – Universitätsmedizin Berlin, Berlin, Germany⁶Institute of Neuropathology, Faculty of Medicine, University of Freiburg, Freiburg, Germany⁷Institute for Medical Microbiology, Immunology and Hygiene, Technische Universität München, Munich, Germany⁸Institute for Pharmacology and Clinical Pharmacy, Philipps-Universität Marburg, Marburg, Germany⁹Groningen Research Institute of Pharmacy, Department of Molecular Pharmacology, Faculty of Science and Engineering, University of Groningen, Groningen, The Netherlands¹⁰Institute for Medical Microbiology and Hospital Hygiene, Philipps University of Marburg, Marburg, Germany¹¹Department of Neurology, Philipps University of Marburg, Marburg, Germany¹²Institute for Molecular Medicine, University Medical Center of the Johannes Gutenberg University Mainz, Mainz, Germany¹³Cologne Excellence Cluster on Cellular Stress Responses in Aging-Associated Diseases (CECAD), University of Cologne, Cologne, Germany¹⁴Institute of Medical Statistics and Computational Biology, Faculty of Medicine, University of Cologne, Cologne, Germany¹⁵Center for Basics in NeuroModulation (NeuroModulBasics), Faculty of Medicine, University of Freiburg, Freiburg, Germany¹⁶Signalling Research Centres BLOSS and CIBSS, University of Freiburg, Freiburg, Germany**Correspondence**

Thorsten Buch, Institute of Laboratory Animal Science, University of Zurich, 8952 Schlieren, Switzerland.

Email: thorsten.buch@uzh.ch

Present address

Giuseppe Locatelli, Novartis Institutes for BioMedical Research (NIBR), Basel, Switzerland.

Abstract

In the central nervous system (CNS), insulin-like growth factor 1 (IGF-1) regulates myelination by oligodendrocyte (ODC) precursor cells and shows anti-apoptotic properties in neuronal cells in different in vitro and in vivo systems. Previous work also suggests that IGF-1 protects ODCs from cell death and enhances remyelination in models of toxin-induced and autoimmune demyelination. However, since evidence remains controversial, the therapeutic potential of IGF-1 in demyelinating CNS

Abbreviations: CNS, central nervous system; EAE, experimental autoimmune encephalomyelitis; IGF-1, insulin-like growth factor 1; IGF1R, insulin-like growth factor receptor 1; IGFBP, IGF-binding protein; MBP, myelin basic protein; MOG, myelin oligodendrocyte glycoprotein; MS, multiple sclerosis; ODC, oligodendrocyte; PLP, proteolipid protein.

This is an open access article under the terms of the [Creative Commons Attribution](https://creativecommons.org/licenses/by/4.0/) License, which permits use, distribution and reproduction in any medium, provided the original work is properly cited.

© 2022 The Authors. *GLIA* published by Wiley Periodicals LLC.

Barbara Ingold-Heppner, Institute of Pathology, DRK Kliniken Berlin, Berlin, Germany.

Funding information

Swiss Staatssekretariat für Bildung und Forschung SBF, Grant/Award Number: COST action BM0603 NEURINFNET; Swiss National Foundation, Grant/Award Number: SNF 310030_197652/1; German Research Foundation DFG, Grant/Award Number: TR22; Swiss Multiple Sclerosis Society, Grant/Award Numbers: 2021-07, 2021-02; Hertie Foundation, Grant/Award Number: P1150013; Bonnizzi-Theler Foundation; Scherbarth Foundation; ARSEP foundation; Sobek Foundation, the Ernst Jung Foundation, the Novo Nordisk Prize, the DFG SFB992, Grant/Award Number: Project ID 192904750; SFB1160, Grant/Award Number: Project ID 256073931; NeuroMac, Grant/Award Number: Project ID 259373024; DFG under Germany's Excellence Strategy, Grant/Award Number: CIBSS-EXC-2189-Project ID 390939984; Reinhart-Koselleck-Grant, Grant/Award Number: Project ID 279642606; Gottfried Wilhelm Leibniz Prize; Alzheimer Forschung Initiative e.V. (AFI); Ministry of Science, Research and Arts, Baden-Wuerttemberg (Sonderlinie "Neuroinflammation"); DFG, Grant/Award Number: CRC1479 (Project ID 441891347); DFG-funded CRC/TRR167 "NeuroMac"; DFG CRC1479, Grant/Award Number: Project ID 441891347

conditions is unclear. To finally shed light on the function of IGF1-signaling for ODCs, we deleted insulin-like growth factor 1 receptor (IGF1R) specifically in mature ODCs of the mouse. We found that ODC survival and myelin status were unaffected by the absence of IGF1R until 15 months of age, indicating that IGF-1 signaling does not play a major role in post-mitotic ODCs during homeostasis. Notably, the absence of IGF1R did neither affect ODC survival nor myelin status upon cuprizone intoxication or induction of experimental autoimmune encephalomyelitis (EAE), models for toxic and autoimmune demyelination, respectively. Surprisingly, however, the absence of IGF1R from ODCs protected against clinical neuroinflammation in the EAE model. Together, our data indicate that IGF-1 signaling is not required for the function and survival of mature ODCs in steady-state and disease.

KEYWORDS

demyelination, EAE, insulin-like growth factor 1, multiple sclerosis, neuroinflammation, oligodendrocyte

1 | INTRODUCTION

Insulin-like Growth Factor 1 (IGF-1) and its receptor (IGF1R) are major regulators of cellular differentiation, growth, motility, and apoptosis (Fernandez & Torres-Aleman, 2012; Floyd et al., 2007; Mason et al., 2003; Pang et al., 2007). The activity of IGF-1 is tightly regulated by a complex system of IGF-binding proteins (IGFBPs) and IGFBP-proteases, determining IGF-1 stability and localization (Adams et al., 2000). In the central nervous system (CNS), IGF1R is expressed by virtually all resident cells (Anlar et al., 1999), and its ligand is both locally produced by glial cells and imported to the CNS from the bloodstream (Fernandez & Torres-Aleman, 2012). IGF-1 is a strong anti-apoptotic factor (Fernandez & Torres-Aleman, 2012; Vincent et al., 2004) and has shown a consistent neuroprotective effect in mouse models of X-linked adrenoleukodystrophy (Mastroeni et al., 2009), A β -induced pathology (Carro et al., 2002), Rett Syndrome (Tropea et al., 2009), and amyotrophic lateral sclerosis (ALS) (Nagano et al., 2005). This molecule has therefore become a strong drug candidate for different pathologies of the CNS (Arpa et al., 2011; Pini et al., 2012; Sevigny et al., 2008); accordingly, the IGF-1 axis has also been investigated in multiple sclerosis (MS) and its animal model experimental autoimmune encephalomyelitis (EAE). Sera from MS patients show lower IGF-1 bioavailability (Lanzillo et al., 2011; Shahbazi et al., 2017) while surviving ODCs upregulate IGF-1, IGF1R, and IGFBP-1/-6 at the edges

of chronically demyelinated plaques (Wilczak et al., 2008). Meanwhile, animal studies using the EAE model display contradicting results. While in some studies IGF-1 administration failed to protect mice from EAE (Cannella et al., 2000; Genoud et al., 2005), or even increased disease severity (DiToro et al., 2020; Lovett-Racke et al., 1998), in other studies it ameliorated clinical outcome (Bilbao et al., 2014), improved remyelination (Li et al., 1998; Liu et al., 1995) and reduced lesions (Yao et al., 1995). The encouraging data from preclinical development led to a clinical study with MS patients. The treatment with IGF-1 was well-tolerated but lacked a therapeutic effect (Frank et al., 2002). However, results from animal studies and clinical trials are difficult to interpret: IGF-1 affects different parenchymal cells and infiltrating inflammatory cells in a cell- and context-specific fashion (Bilbao et al., 2014; Cuscik et al., 2014; DiToro et al., 2020; O'Donnell et al., 2002). Along these lines, even though the IGF-1/IGF1R axis is a known regulator of survival, proliferation and myelination by ODC progenitors (OPCs) (Beck et al., 1995; Carson et al., 1993; D'Ercole et al., 2002; Pang et al., 2007; Zeger et al., 2007), the function of IGF1R signaling in mature, post-mitotic ODCs remains controversial (Cheng et al., 1998; Mason et al., 2003; Ye et al., 2002). This lack of knowledge impedes further therapeutic approaches on the IGF axis and interpretation of clinical results in MS.

In the current study, we assessed the role of IGF-1 in mature ODCs by using a mouse model which overcomes the limitations of



IGF-1 application or developmental ablation of IGF1R. We limited genetic IGF1R ablation to mature myelin oligodendrocyte glycoprotein (MOG)-expressing ODCs and showed that signaling through the IGF1R does not regulate survival of ODCs or myelin status during aging, toxin-induced demyelination, and neuroinflammation. The absence of IGF1R from ODCs led to unexpected protection from the induction of EAE and an intrinsically ameliorated disease. Altogether, our results suggest cell-specific beneficial effects of reduced IGF-1 signaling in the context of neuroinflammation.

2 | RESULTS

2.1 | Deletion of IGF1R from mature ODCs does not affect ODC number and myelin status

First, to understand whether ODCs express IGF1R in the homeostatic human brain and during MS, we analyzed mRNA levels in an existing single-nucleus RNA sequencing dataset obtained from post-mortem human brains of patients without and with MS (Jäkel et al., 2019). We observed expression of the IGF1R in all ODCs and OPCs of healthy and inflamed tissue (Figure 1a). Further, increased expression was found in the committed oligodendrocyte (COPs) cluster of chronic inactive lesions and the oligo6 cluster of remyelinating lesions, suggesting a key function of IGF1R in ODC development (Jäkel et al., 2019). Next, to functionally study the role of IGF-1 signaling in mature ODCs, we moved to a mouse model. We crossed a strain carrying a loxP-flanked 3rd exon of the *IGF1R* gene (Klötting et al., 2008), coding for the ligand-binding moiety, to the *MOG-cre* strain (Hovelmeyer et al., 2005) displaying Cre activity in post-mitotic mature ODCs; we hereafter call these animals *oIGF1R^{-/-}* mice (Figure 1b). In contrast to previously published models using *Olig1*- and *PLP-cre* (Zeger et al., 2007), the deletion of IGF1R in *oIGF1R^{-/-}* mice did not affect developmental myelination as the promoter for MOG commences expression in ODCs at the terminal stage of myelination (Solly et al., 1996), as we previously described (Locatelli et al., 2012; Locatelli et al., 2015). By using the genotyping approach reported in Klötting et al., 2008, we observed recombination of the loxP-flanked *Igf1r* gene specifically in CNS and not in peripheral tissue (i.e., tail) of *oIGF1R^{-/-}* mice (Figure 1c). A more detailed analysis on upper and lower spinal cord, hippocampus, cerebellum, spleen, kidney, and liver confirmed tissue specificity (data not shown). To assess the degree of *MOG-cre*-driven recombination in *oIGF1R^{-/-}* mice and better characterize the frequency of cre-mediated genetic recombination in mature ODCs, we crossed *MOG-cre* mice to a fluorescent reporter strain (*ROSA26-EYFP*) (Srinivas et al., 2001). We found that in these *oIGF1R^{EYFP}* reporter mice, EYFP was expressed by 98% of CC1⁺ ODCs in the cortex and cerebellum and 67% of CC1⁺ ODCs in the spinal cord (Supplementary Figure 1a,b). To obtain information about the deletion frequency on the basis of individual ODCs, we analyzed IGF1R expression by immunofluorescence analysis of CNS tissue sections. We confirmed that, compared to mature CC1⁺ ODCs in Cre-negative littermates, most ODCs in the *oIGF1R^{-/-}* brain and spinal cord did not express IGF1R (Figure 1d,e). Together, characterization

of Cre-induced recombination in *oIGF1R^{-/-}* mice indicated an efficient deletion of IGF1R from mature ODCs.

We next assessed whether the absence of IGF-1 signaling in ODCs leads to changes in weight, basic micro-anatomy, and motor function. Analysis of the CNS of *oIGF1R^{-/-}* mice by H&E staining, LFB-PAS staining, and through Iba1-specific antibodies failed to reveal structural and cellular anomalies or signs of gliosis (Supplementary Figure 1c). Furthermore, *oIGF1R^{-/-}* mice did not show any difference in body weight compared to controls (Supplementary Figure 1d). We used a Rotarod test for assessing motor function and did not observe any impediments until 15 months of age (Supplementary Figure 1e).

As IGF-1 signaling is known to regulate myelination in ODC progenitors (Wrigley et al., 2017), we next assessed the overall myelin content of the CNS of *oIGF1R^{-/-}* and control mice at 3, 5, and 9 months of age by immunoblotting. Western blot analysis did not reveal any significant differences in protein levels of MOG and myelin basic protein (MBP) (Supplementary Figure 2a-c). To exclude the possibility of regional changes of myelin content through IGF1R ablation, we performed a detailed histological analysis of PLP expression. Again we did not find any difference in the myelination of white matter tracts of *oIGF1R^{-/-}* mice compared to controls, with myelin sheaths appearing uncompromised up to at least 15 months of age (Figure 2a,b and data not shown).

Further, ultrastructural analysis by electron microscopy did not reveal ultrastructural abnormalities in ODCs in 1 month and 12 months-old animals (Figure 2c,d). Also a g-ratio analysis in 1 year old animals did not show any difference between groups (Supplementary Figure 2d). Accordingly, and in contrast to reported developmental ablation of IGF1R along ODC maturation (Zeger et al., 2007), ODC density was unchanged in the CNS of *oIGF1R^{-/-}* mice compared to controls (Figure 2e and Supplementary Figure 2e). Next, we investigated whether the density of NG2⁺ OPCs would also remain unaltered in *oIGF1R^{-/-}* mice. Interestingly, while the number of NG2⁺ OPCs in tissue sections was comparable to littermate controls in most CNS regions, we detected an increased number of NG2⁺ cells specifically in the brain stem of 9 months old *oIGF1R^{-/-}* mice (Figure 2f,g), thus indicating that prolonged absence of IGF1R can have local indirect effects on the OPC lineage during aging. Analysis of axonal structures by NF staining and electron microscopy did not show differences between *oIGF1R^{-/-}* and controls (Supplementary Figure 2f,g and data not shown). Taken together, absence of IGF1R signaling in mature ODCs did not lead to major CNS abnormalities in young and aged mice.

2.2 | IGF1R signaling does not affect ODC survival during toxic demyelination

The copper chelator cuprizone is a widely used agent for investigating non-inflammatory sterile demyelination and subsequent remyelination. It leads to mitochondrial impairment in ODC (Benetti et al., 2010; Werner et al., 2010) and subsequent transient depletion of ODCs mainly from the corpus callosum (Zatta et al., 2005). Given the described myelo-protective role of IGF-1 in the cuprizone model

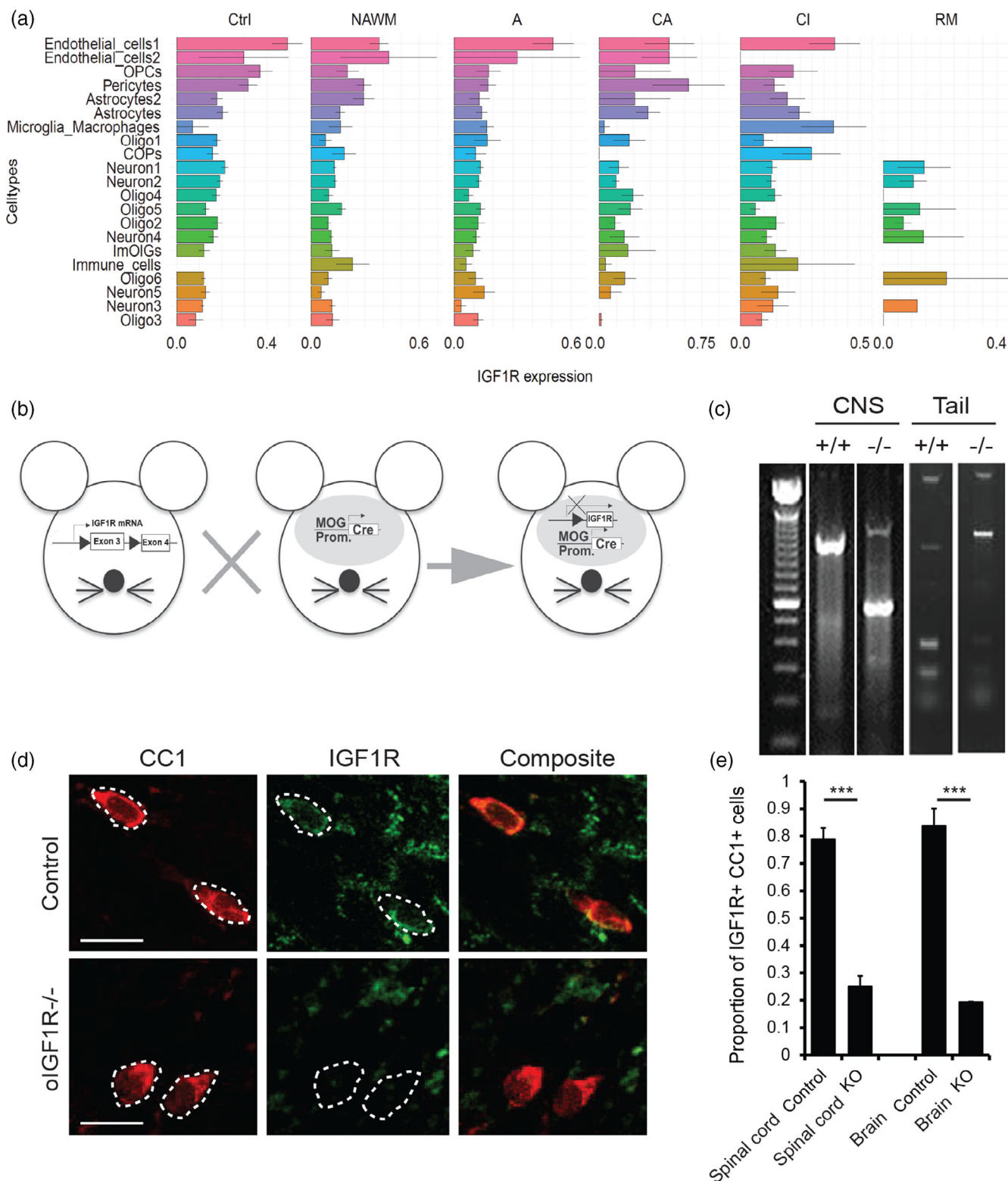


FIGURE 1 Legend on next page.

(D'Ercole et al., 2002; Mason et al., 2000), we tested the sensitivity of IGF1R-negative ODC toward toxin-induced degeneration. Feeding of *oIGF1R*^{-/-} and control mice with 0.2% cuprizone led to both comparable ODC depletion and subsequent repopulation in the two groups (Figure 3a). We were also unable to find differences in animal

weight (Supplementary Figure 3a) and in the histological appearance of the corpus callosum (Supplementary Figure 3b). Analyses of PLP and MOG protein levels by western blot (Figure 3b,c) and histology (Figure 3d) revealed no significant differences between groups. As demyelination leads to the accumulation of progenitors of ODCs, we



analyzed the density of OPCs in the corpus callosum and observed similar accumulation of NG2⁺ cells in the mutant animals following cuprizone intoxication (Figure 3e,f). Also, analysis of the axonal status by NF- and Smi32-specific staining did not reveal differences between the genotypes (Figure 3g,h). In summary, the absence of IGF1R from mature ODCs during cuprizone-induced demyelination, hence mitochondrial stress, did not have an impact on the survival of ODCs nor affect the timing of remyelination following toxin removal.

2.3 | Diminished neuroinflammation in *oIGF1R*^{-/-} mice compared to controls

The cellular and molecular mechanisms leading to demyelination in neuroinflammation differ substantially from cuprizone-intoxication and include oxidative stress, excitotoxicity, CD8⁺ T cell cytotoxicity, and stimulation of death receptors (McTigue & Tripathi, 2008). However, the role of IGF-1-mediated signaling in protecting ODCs during neuroinflammation has remained controversial (Bilbao et al., 2014; Cannella et al., 2000; DiToro et al., 2020; Genoud et al., 2005; Lovett-Racke et al., 1998). We hence addressed whether IGF1R signaling was involved in the response of mature ODCs to autoimmune CNS inflammation and induced EAE by immunizing *oIGF1R*^{-/-} mice and *oIGF1R*^{+/+} controls against the MOG₃₅₋₅₅ peptide. Surprisingly, we consistently observed less severe development of clinical neuroinflammation by ablation of IGF1R. Disease incidence (91.3% in control *oIGF1R*^{+/+} mice vs. 69.2% in *oIGF1R*^{-/-}) and clinical severity both significantly decreased (Figure 4a,b). While the *oIGF1R*^{+/+} control groups in these EAE experiments did not comprise *cre*⁺ animals (Supplementary Figure 4a), further tests comparing disease development in *MOG-cre*⁺ and *MOG-cre*^{negative} mice excluded a potential *Cre*- or *Mog*-locus-dependent bias in EAE outcome (Supplementary Figure 4b).

To investigate whether priming of the immune response against the MOG peptide differed between *oIGF1R*^{-/-} and control animals, we assessed the number of antigen-specific T cells in mice immunized with MOG₃₅₋₅₅. We performed an *in vitro* restimulation with the peptide and found a comparable response for all

genotypes (Supplementary Figure 4c). Since a decreased number of regulatory Foxp3⁺ T (Treg) cells was reported to lead to enhanced EAE severity (Koutouros et al., 2014) we compared Treg cell numbers in both genotypes. Accordingly, the numbers of Treg cells were unaffected by absence of IGF1R on ODCs in the induction phase of EAE in lymph nodes (Supplementary Figure 4d). To investigate the underlying transcriptomic differences as a result of the absence of IGF1R from ODCs, we performed microarray analysis of spinal cord tissue of immunized mice 9 days p.i. (pre-clinical phase). However, this analysis revealed no relevant and significant differences between *oIGF1R*^{-/-} and control mice (data not shown). In conclusion, the absence of IGF1R from mature ODCs decreased the clinical severity and incidence of EAE without directly affecting the T cell response.

2.4 | IGF1R does not control ODC number or apoptosis during EAE

To unmask the distinct role of IGF1R from overlying effects of the observed severity of EAE in individual mice, we performed a detailed histological analysis in time- and clinical score-matched *oIGF1R*^{-/-} and control animals. We did not observe any relevant histopathological differences after H&E and LFB-PAS stainings and by ultrastructural analysis (data not shown). Notably, ODC density in the different experimental groups remained unchanged at peak EAE and after 1 month of disease (Figure 4c). Similarly, the level of myelin proteins such as MBP and MOG was comparable in *oIGF1R*^{-/-} mice compared to control mice (Figure 4d). To investigate whether IGF1R plays an anti-apoptotic role in ODCs during EAE, we then analyzed the number of apoptotic CC1⁺ cells in the acutely inflamed spinal cord through staining for activated Caspase 3 (Casp3) (Supplementary Figure 5a). Both, the densities of Casp3⁺ CC1⁺ cells and the total number of Casp3⁺ cells appeared comparable in *oIGF1R*^{-/-} mice compared to controls (Figure 4e,f), thus showing that the absence of IGF1R from ODCs did not have a general influence on ODC apoptosis during EAE. We next analyzed whether recruitment of progenitors of ODCs was affected in *oIGF1R*^{-/-} and found a comparable accumulation of NG2⁺ OPCs in the inflamed

FIGURE 1 Expression of IGF1R in human and mouse ODCs, and receptor deletion in *oIGF1R*^{-/-} mice. (a) Expression of *IGF1R* by the indicated cell types from MS patients and healthy individuals. Single cell RNAseq data as published by Jäkel et al. (Jäkel et al., 2019). Ctrl, nuclei from healthy individuals; from MS patients: NAWM, normal-appearing white matter; A, active; CA, chronic active; CI, chronic inactive; RM, remyelinated. (b) Mice carrying an IGF1R gene with loxP-flanked 3rd exon (*IGF1R*^{fl/fl}, left) were crossed to mice expressing the Cre recombinase specifically in ODCs (*MOG*^{i-cre}, center). The resulting offspring (*MOG*^{i-cre}^{Tg/WT}/*IGF1R*^{fl/fl} = *oIGF1R*^{-/-}) features recombination of the IGF1R locus specifically in MOG-expressing, mature ODCs. (c) DNA was isolated from CNS and tails of *oIGF1R*^{-/-} and control animals. PCR with primers spanning exon 3 of the IGF1R gene reveals bands of 1100 bp (WT gene) in *IGF1R*^{+/+} control mice and bands of 1350 bp (*IGF1R*^f allele) and 570 bp (*IGF1R*^d allele/recombined locus) in *oIGF1R*^{-/-} mice. Recombination of the *IGF1R*^f allele was specific for the CNS. (d) Representative picture of spinal cord white matter sections from *oIGF1R*^{-/-} and control animals immunostained with the ODC-specific CC1 and with IGF1R-specific antibodies. CC1 is shown in red, IGF1R in green. Dashed white lines indicate CC1⁺ ODCs highlighting the IGF1R negativity of ODCs in *oIGF1R*^{-/-} mice. Scale bar, 30 μm. (e) Quantification of IGF1R-expressing CC1 positive cells in brain and spinal cord isolated from *oIGF1R*^{-/-} and control mice, following manual blinded quantification of immunofluorescent staining for pIGF1R and CC1, for brain *n* = 3, for spinal cord *n* = 6. Two tailed student's T test, *** = *p* < .001. A, active; CA, chronic active; CI, chronic inactive; CNS, central nervous system; MOG, myelin oligodendrocyte glycoprotein; MS, multiple sclerosis; NAWM, normal-appearing white matter; ODC, oligodendrocyte; RM, remyelinated

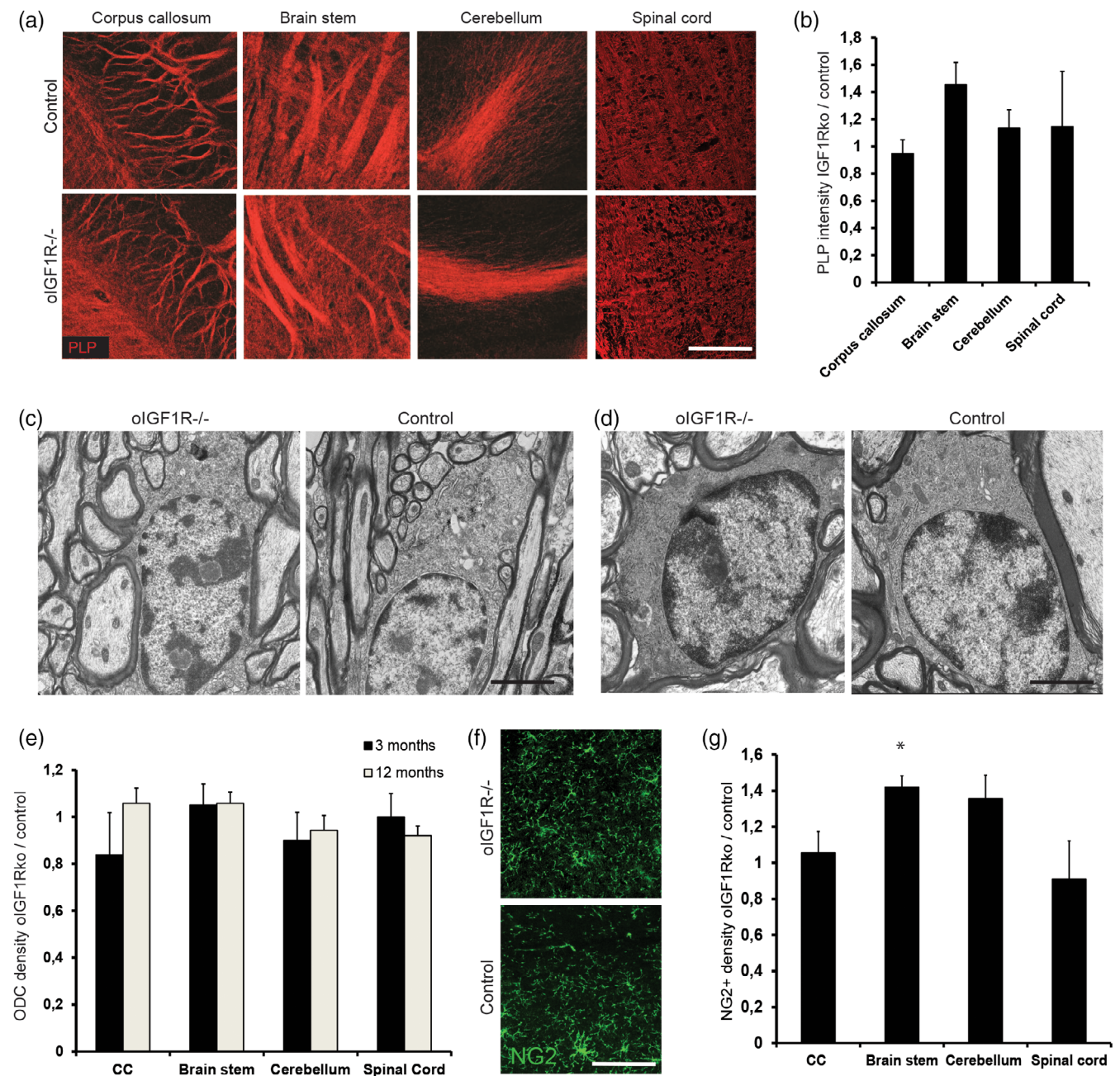


FIGURE 2 Absence of IGF1R from mature ODC does not lead to structural or cellular abnormalities in the CNS. (a) CNS sections from $oIGF1R^{-/-}$ and control mice of 1 month of age were stained with a PLP-specific antibody (displayed in red). Scale bar, 200 μ m. (b) Relative intensity of PLP-specific staining from sections treated as in (a). Shown is mean \pm s.e.m., $n = 5$. (c) Representative electron micrographs of ODCs and myelinated axons from the cerebellum of 1 month old and (d) 12 months old $oIGF1R^{-/-}$ and control mice. (e) Sections from indicated CNS areas $oIGF1R^{-/-}$ and control mice at 3 or 12 months of age were immunostained with an ODC-detecting, ASPA-specific antibody. Cells were manually counted in a blinded fashion; shown is the relative ASPA⁺ cell density in $oIGF1R^{-/-}$ compared to control mice. The bar graph depicts the mean density \pm s.e.m., $n = 5$. (f) Representative sections of the brain stem of 9 months old $oIGF1R^{-/-}$ and control mice were immunostained with the OPC-detecting NG2-specific antibody. Scale bar, 50 μ m. (g) CNS sections from 9 months old $oIGF1R^{-/-}$ and control mice were immunostained with NG2-specific antibodies and cells manually counted (field size: 0.25 mm [Floyd et al., 2007]). The bar graph shows relative cell density \pm s.e.m., $n = 4$. * $p < .05$, Student's T test. ASPA, aspartoacylase; CNS, central nervous system; IGF1R, insulin-like growth factor receptor 1; ODC, oligodendrocyte; PLP, proteolipid protein

spinal cords of $oIGF1R^{-/-}$ and control mice (Supplementary Figure 5b). Also, the density of NeuN⁺ neurons was similar in the spinal cord of the different experimental groups (Figure 4g and

Supplementary Figure 5c), and ultrastructural investigation of axonal status in the white matter nearby inflammatory lesions did not reveal any obvious difference between groups (data not shown). Taken

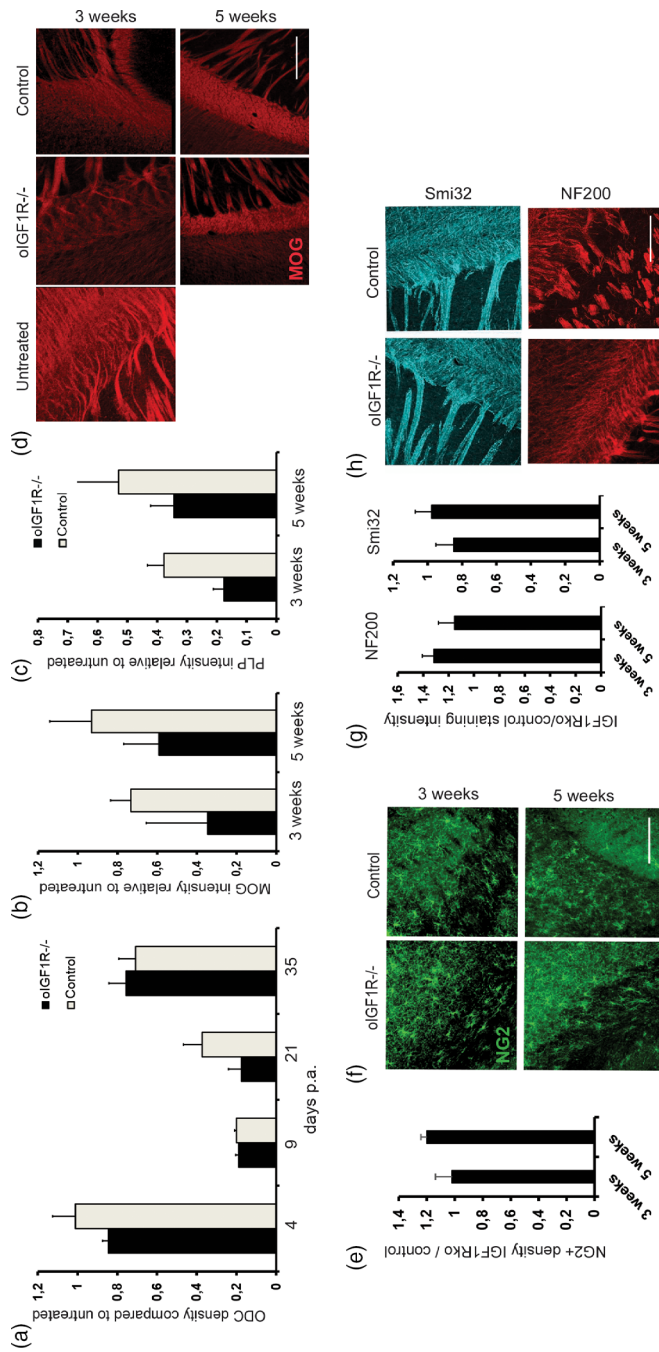


FIGURE 3 ODC loss and demyelination following cuprizone intoxication. (a) *oIGF1R^{-/-}* and control mice were fed with 0.2% cuprizone and sacrificed at days 4, 9, 21, and 35 after treatment start. Sagittal sections of the corpus callosum were immunostained for ASPA and cells counted manually and blinded. The values are relative to control mice which did not receive cuprizone. The bar graph shows mean density \pm s.e.m., $n = 5$. (b and c) Mice were fed with 0.2% cuprizone and sacrificed after 3 or 5 weeks. Brain lysates were immunoblotted and analyzed using MOG- (b) and PLP-specific (c) antibodies. Values are relative to control mice, which did not receive cuprizone in the diet. The bar graph shows mean intensity \pm s.e.m., $n = 4$. (d) *oIGF1R^{-/-}* and control mice were sacrificed 3 and 5 weeks after cuprizone feeding and sagittal sections of the corpus callosum were stained with MOG-specific antibodies. As controls served mice which did not receive cuprizone. Scale bar, 200 μ m. (e) Mice were treated as in (a). Sagittal sections of the corpus callosum were immunostained for NG2 and cells counted manually in a blinded fashion (field size: 0.12 mm [Floyd et al., 2007]). Bar graph shows mean \pm s.e.m., $n = 5$. * $p < .05$, two tailed Student's T test. (f) Representative sections of the corpus callosum of *oIGF1R^{-/-}* and control mice 3 and 5 weeks after beginning of cuprizone treatment, immunostained with NG2-specific antibody. Scale bar, 200 μ m. (g) Mice were treated as in (a). Sagittal sections of the corpus callosum were immunostained with the neuronal cytoskeleton marker NF200- and non-phosphorylated neurofilament Smi32-specific antibodies and the staining intensity quantified. The bar graph shows mean \pm s.e.m., $n = 4$. (h) Representative sagittal sections of the corpus callosum of *oIGF1R^{-/-}* and control mice 3 and 5 weeks after beginning of cuprizone treatment immunostained with NF200- and Smi32-specific antibodies. Scale bar, 200 μ m. ASPA, aspartoacylase; CNS, central nervous system; IGF1R, insulin-like growth factor receptor 1; ODC, oligodendrocyte glycoprotein; PLP, proteolipid protein

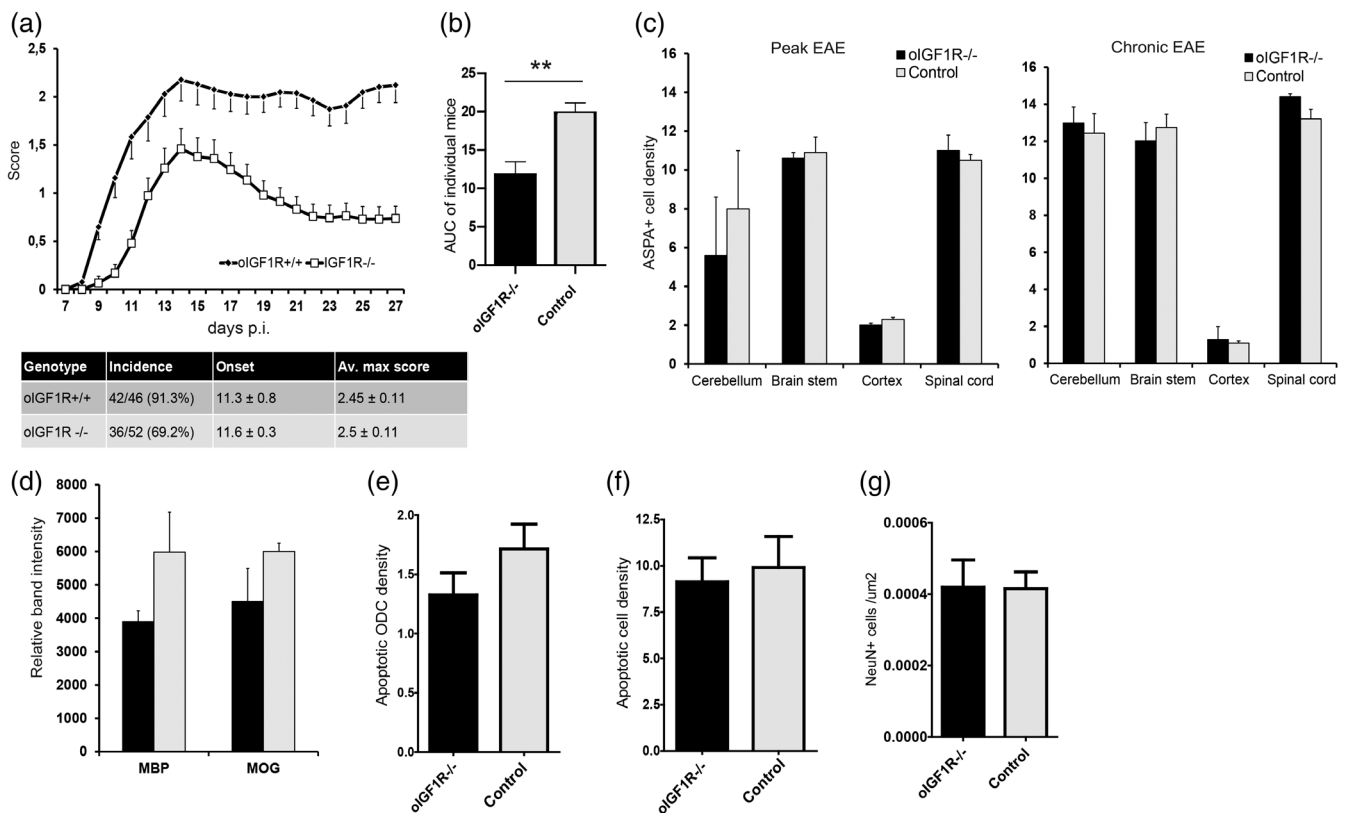


FIGURE 4 *oIGF1R*^{-/-} mice show ameliorated disease but no change in ODC density. (a) *oIGF1R*^{-/-} and control animals were induced with EAE and scored daily for clinical signs of disease. Shown is clinical score of disease and a table reporting incidence, day of clinical onset and average maximum clinical score. The data was pooled from 6 independent EAE experiments (total of 52 *oIGF1R*^{-/-} and 46 control mice). (b) Area under the curve (AUC) calculation of disease severity in the mice shown in (a), shown is average ± s.e.m. ***p* < .001, Mann Whitney U test. (c) *oIGF1R*^{-/-} and control mice were induced with EAE and sacrificed at peak disease and 1 month (Chronic EAE) after induction of EAE. CNS sections were immunostained with ASPA-specific antibody and cells manually counted in a blinded fashion (field size 0.22 mm [Floyd et al., 2007]). The data is representative of two independent experiments. The bar graph shows mean ± s.e.m., *n* = 9. (d) Brain lysates of *oIGF1R*^{-/-} and control mice 1 month after induction of EAE were immunoblotted and analyzed using MOG- and MBP-specific antibodies. The bar graph shows mean staining intensity ± s.e.m., *n* = 5. (e) Spinal cord sections of *oIGF1R*^{-/-} and control mice 2 days after clinical onset of EAE were stained with DAPI, CC1 and activated caspase 3-specific antibodies. The number of CC1⁺ Casp3⁺ cells or (f) Casp3⁺ cells, manually counted in a blinded fashion (field size 0.25 mm [Floyd et al., 2007]), is shown. The data is representative of two independent experiments. The bar graph shows the mean number ± s.e.m., *n* = 7. (g) NeuN⁺ cells manually counted (field size 0.25 mm [Floyd et al., 2007]). Data are representative of two independent experiments. Bar graph shows average number ± s.e.m., *n* = 7. ASPA, aspartoacylase; CNS, central nervous system; EAE, experimental autoimmune encephalomyelitis; IGF1R, insulin-like growth factor receptor 1; ODC, oligodendrocyte; MBP, myelin basic protein; MOG, myelin oligodendrocyte glycoprotein

together, deletion of IGF1R from mature ODCs did not affect ODC survival within neuroinflammatory lesions.

2.5 | Absence of IGF1R from ODCs does not impact inflammation upon EAE development

To dissect the underlying mechanisms of amelioration of EAE development in the absence of IGF1R signaling, we analyzed recruitment of peripheral immune cells into the CNS and the local glia response to inflammation. Histological analysis revealed comparable lesion size between *oIGF1R*^{-/-} and control mice (Supplementary Figure 5d). By flow cytometry, we observed that the total number of invading lymphocytes in the CNS was not different between clinical score-matched *oIGF1R*^{-/-} and controls, both at the peak of the disease and during the chronic phase (Figure 5a).

Furthermore, the production of key inflammatory cytokines such as IFN- γ , GM-CSF, and IL-17 by invading CD4⁺ T cells did not differ between groups at the peak of the disease (Supplementary Figure 6a, Figure 5b), neither in the percentage of expressing cells nor in expression level per cell population (data not shown). Also, the number of CNS-infiltrating Treg cells was comparable among the different groups (Figure 5c). Both, by histological examination and by flow cytometry, we observed similar numbers of microglia and invading macrophages in *oIGF1R*^{-/-} and control animals, with a comparable MHC-II expression (Figure 5d-f). Furthermore, both CD11b^{high}CD45^{high} invading myeloid cells and CD11b^{intermediate}CD45^{intermediate} microglia showed similar expression of the markers CD11c, CD95, CD95I, and CD44, with subtle expression variations, showing statistical significance only in case of CD44 positivity by invading macrophages (Figure 5f).

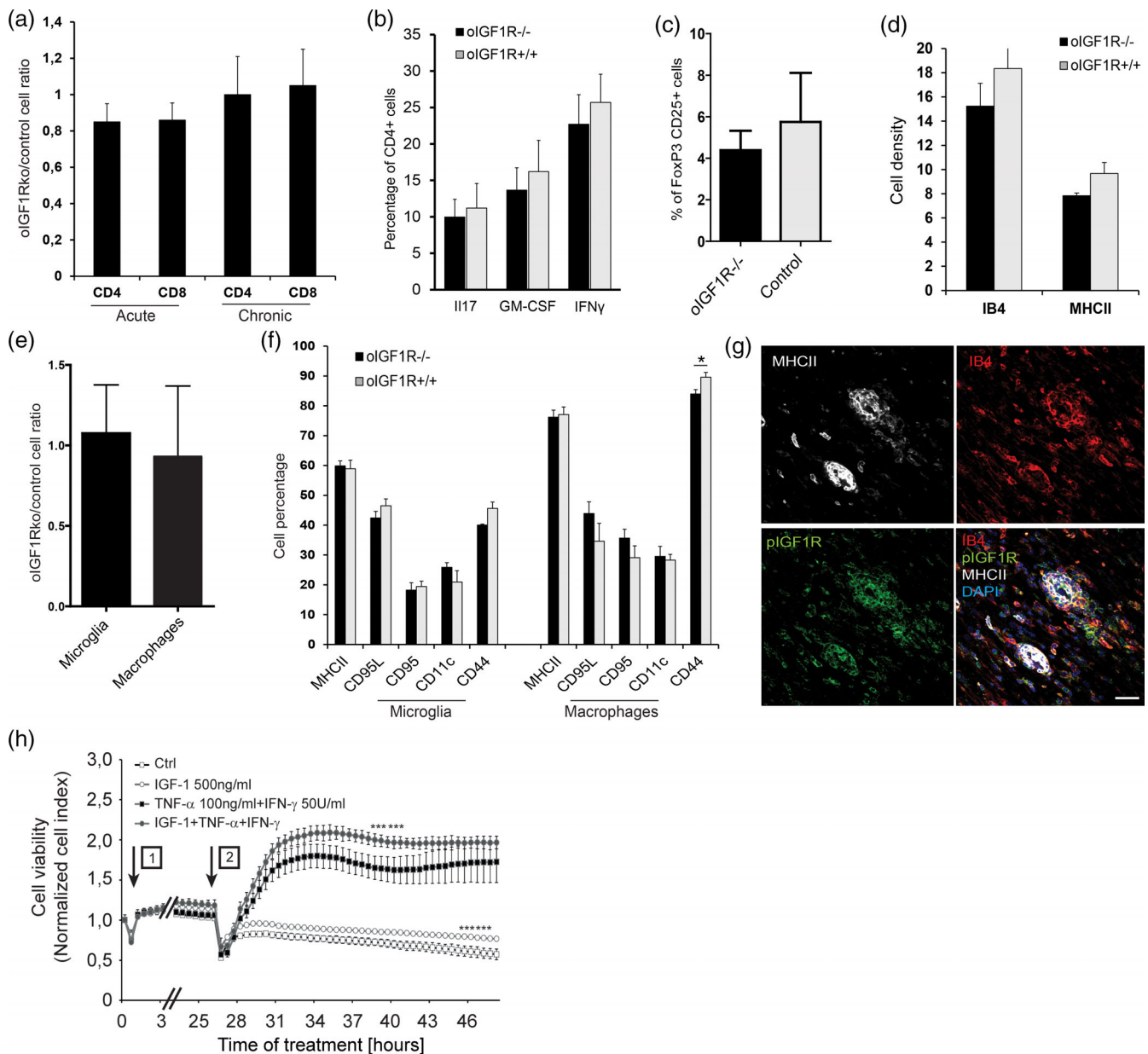


FIGURE 5 Legend on next page.

Notably, immunofluorescent analysis of IGF1R expression at the clinical peak of EAE revealed a strong expression by microglia/macrophages (data not shown), especially within inflammatory lesions in MHC-II $^{+}$ cells (Figure 5g). To assess whether IGF1R signaling might directly impact the functioning of myeloid cells in our model, we assessed the effect of IGF-1 signaling on microglia proliferation in vitro (Dolga et al., 2012). We observed that treatment of microglial cells with IGF-1 (500 ng/ml) in vitro led to an increase in the proliferation rate under standard culture conditions and following TNF- α and IFN- γ -mediated activation (Figure 5h, Supplementary Figure 6b,c), but did not alter the expression levels of the activation markers MHC-II and CD44 (Supplementary Figure 6d,e).

Taken together, despite a significant reduction in EAE clinical course, histological and cytometric analysis of CNS inflammation

only revealed minor changes due to the absence of IGF1R from ODCs.

3 | DISCUSSION

Once considered mere myelinating cells of the CNS, the central importance of ODCs in CNS homeostasis and pathological disturbances have found ever greater appreciation in recent years. ODCs were described to provide essential metabolic support for CNS axons and thus proved to be vital for regular neuronal activity (Funfschilling et al., 2012; Lee et al., 2012). These functional connections were supported further in a recent study showing the loss of temporal resolution of axonal signaling upon induction of metabolic defects in ODCs

(Moore et al., 2020). Furthermore, experimental ODC ablation (Locatelli et al., 2012), ODC-specific peroxisome impairment, and PLP overexpression (Ip et al., 2006; Kassmann et al., 2007) were invariably followed by neuronal degeneration. Notably, in the two latter genetically-modified models, ODC impairment also led to the recruitment of lymphocytes to the CNS (Ip et al., 2006; Kassmann et al., 2007), thus indicating that ODCs participate in the complex interplay between the CNS and the immune system (Kerschensteiner et al., 2009; Zeis & Schaeren-Wiemers, 2008).

The key role of ODCs in CNS homeostasis becomes particularly relevant in MS and is well-represented in demyelinating animal models such as EAE (Locatelli et al., 2012; Lucchinetti et al., 1999; McTigue & Tripathi, 2008) and cuprizone intoxication (Benetti et al., 2010; Zatta et al., 2005). In EAE, ODC death and demyelination within CNS inflammatory lesions are central to the clinical progression of disease (Lucchinetti et al., 1999). ODCs in MS patients also show altered heterogeneity that may suggest susceptibility to demyelination and epigenetic differences in genes such as *BCL2L2* and *NDRG1* potentially decreasing anti-apoptotic mechanisms even in non-affected CNS regions (Huyhn et al., 2014; Jäkel et al., 2019). However, finding suitable therapeutic strategies protecting ODCs and myelin during neuroinflammation and other CNS diseases is a relatively untapped research area. The IGF-1 pathway has been among those protective strategies assessed in recent years in MS and its model EAE, but results remained sadly inconsistent among studies (Bilbao et al., 2014; Cannella et al., 2000; DiToro et al., 2020; Genoud et al., 2005; Lanzillo et al., 2011; Li et al., 1998; Liu et al., 1995; Lovett-Racke et al., 1998; Shahbazi et al., 2017; Wilczak et al., 2008; Yao et al., 1995). To finally settle the specific question about the role of the IGF-1 pathway during CNS inflammation we decided for

genetically ablating its receptor from mature ODC. In this genetic model, we observed that the presence of IGF1R appeared dispensable for physiological maintenance of myelin and cell survival of mature ODCs in adult animals up to 15 months of age, even though IGF-1 is known to deliver a robust anti-apoptotic signal to OPCs during development (Chesik et al., 2008). While at first sight this result appears to differ from observation in an IGF1R ablation model using PLP-cre, in which the authors showed up to 25% decrease in ODC numbers in the corpus callosum at 25 weeks of age (Zeger et al., 2007), this work also presented IGF1R deletion in a fraction of NG2⁺ OPCs. It hence appears possible that PLP-cre induced recombination partially affected CNS cell-types other than mature ODCs (Michalski et al., 2011). Our study, by using a genetic model restricting recombination most stringently to mature ODCs, and by addressing several timepoints and anatomical CNS regions, leads instead to the firm conclusion that ODC-specific absence of IGF1R does not alter the steady-state physiology of these cells nor CNS myelin status.

Using an inflammatory model of MS and a toxin-induced demyelination model, we further show that absence of IGF1R from mature ODCs: (a) does not alter the pathophysiology of cuprizone-mediated demyelination, (b) does not significantly affect the subsequent remyelination and (c) does not affect the survival of ODCs in neuroinflammatory lesions. Taken together, experiments in *oIGF1R*^{-/-} mice showed unchanged ODC densities during adulthood, aging, cuprizone-intoxication, and EAE, clearly indicating that survival of mature ODCs is not controlled by activation of IGF1R in these contexts. Our data thus suggest that the dependence of ODC lineage cells on the anti-apoptotic function of IGF-1 is lost during terminal differentiation. Such reliance on specific pathways was reported for multiple developmental stages of ODCs. For instance, AMPA/kainate receptor-mediated excitotoxicity

FIGURE 5 Inflammatory cell phenotype during anti-CNS autoimmunity in absence of oligodendroglial IGF1R. (a) Cells from the CNS of *oIGF1R*^{-/-} and control animals 2 days (acute) or 12 days (chronic) after induction onset of EAE were analyzed by flow cytometry. They were stained with CD4-, CD8-, CD11b-, CD45-specific antibodies. Shown is the relative number of CD4⁺ and CD8⁺ T cells in the CD11b^{negative}, CD45⁺ population in *oIGF1R*^{-/-} compared to control mice. The data is representative of two independent experiments, shown is the mean ± s.e.m. ($n = 8$). (b) Bar graph showing percentage of pro-inflammatory cytokine producing T cells in the CD4⁺, CD11b^{negative}, CD45⁺ population isolated from the CNS of *oIGF1R*^{-/-} and control mice induced with EAE and analyzed at peak disease. The data is representative of two independent experiments; shown is the mean ± s.e.m., $n = 8$. (c) Cells were isolated from the spinal cord and cerebellum of *oIGF1R*^{-/-} and control animals 2 days after disease onset (day 12 post immunization) and analyzed by flow cytometry after staining with CD4-, CD11b-, CD45-, Foxp3-specific antibodies. Shown is the total number of Foxp3⁺, CD4⁺, CD11b^{negative}, CD45⁺ cells per CNS ($n = 4$). (d) EAE was induced in *oIGF1R*^{-/-} and control animals and animals sacrificed at clinical peak of disease. Spinal cord sections were stained with DAPI, MHC-II, and IB4-specific antibody and positive cells manually and blindly counted. Shown is the mean ± s.e.m., $n = 4$. (e) *oIGF1R*^{-/-} and control animals were induced with EAE. CNS cells isolated at peak disease and immunostained for CD45, CD11b were analyzed by flow cytometry. Shown are relative percentages per CNS of CD45^{intermediate}-CD11b⁺ microglia and of CD45^{high}-CD11b⁺ activated microglia/macrophages in *oIGF1R*^{-/-} compared to *oIGF1R*^{+/+} controls. The data is representative of three independent experiments. The bar graph shows the mean ± s.e.m., $n = 10$. (f) Cells were isolated at peak disease from the CNS of MOG-immunized *oIGF1R*^{-/-} and control animals. The cells were immunostained for CD45, CD11b, CD11c, CD95I, MHC-II, CD95, and CD44 and analyzed by flow cytometry. Shown are relative percentages. The data is representative of two independent experiments. The bar graph shows mean ± s.e.m., $n = 8$. * $p < .05$, Mann Whitney U test. (g) Spinal cord sections from EAE-induced *oIGF1R*^{-/-} animals 2 days after disease onset were immunostained with DAPI, Isolectin B4, and with MHC-II-, activated IGF1R-specific antibodies. Scale bar, 60 μm . (h) Microglial cells were seeded in 96-well E-plates at a density of 15,000 cells/well and monitored with a real-time impedance-based xCELLigence system. After 24 h, the cells were treated with IGF-1 (500 ng/ml) in the absence of serum in the medium (as indicated with the arrow [Fernandez & Torres-Aleman, 2012]). A short time after each treatment, the cell index drastically drops for 30–60 min due to the media change and temperature difference. The time point of treatment or media change is marked as “0 h” in the graph ($n = 3$). Subsequently, microglia was activated with recombinant mouse (rm)TNF- α 100 ng/ml and rmIFN- γ 50 U/ml in the presence or absence of IGF-1500 ng/ml (as indicated with the arrow [Floyd et al., 2007]). Results are given as mean values ± S.D. (** $p < .001$ vs. non-treated microglia, ANOVA, Scheffé’s test, $n = 3$). ASPA, aspartoacylase; CNS, central nervous system; EAE, experimental autoimmune encephalomyelitis; IGF1R, insulin-like growth factor receptor 1; ODC, oligodendrocyte; MOG, myelin oligodendrocyte glycoprotein

(Benarroch, 2009), anoxia (Khawaja & Volpe, 2008), oxidative stress (French et al., 2009), and IFN- γ signaling (Lin et al., 2007) show stage-specific survival potential for the ODC lineage.

Even though the absence of IGF1R did not affect ODC survival in our model, it consistently lowered disease presentation upon induction of anti-myelin autoimmunity, reducing the incidence of the disease and the severity of affected animals. We show that this protection was not mediated by reduction of the encephalitogenic T cell response. It rather seems to be an inherent property of the IGF1R-deficient ODC compartment. However, when we analyzed mRNA expression in the spinal cord of pre-clinical animals, we did not find any significant difference that could provide an explanation or support further hypothesis-driven exploration. Therefore, the actual mechanism behind EAE amelioration in *oIGF1R*^{-/-} mice remains at this point unclear.

We put forward two non-complementary hypotheses to explain the observed beneficial role of decreased IGF-1 signaling in ODCs during neuroinflammation: (A) The ODC-specific deletion of IGF1R led to a local unbalance in IGF-1 bioavailability, in turn enhancing IGF1R signaling in other cell types within the CNS. While this hypothesis remains challenging to prove experimentally, our *in vitro* culture system provided evidence that IGF-1 directly supports microglia expansion. Similarly, several other blood-borne and CNS parenchymal cell types could be affected by variations in IGF-1 signaling, in turn impacting EAE development (Billbao et al., 2014; DiToro et al., 2020; Labandeira-Garcia et al., 2017). (B) Absence of IGF1R affects the overall metabolic activity of ODCs, leading to an increased stress resistance of these cells. Upon EAE induction this improved resilience turns into the observed decreased clinical disease also by indirectly aiding the performance of axons which are metabolically connected to ODCs (Funfschilling et al., 2012; Lee et al., 2012). This hypothesis is supported by previous observations: IGF1R signaling is a regulator of insulin-like anabolism in the adult CNS in a context-dependent manner (Cheng et al., 1998; Fernandez & Torres-Aleman, 2012). Lower metabolic rates in IGF1R^{KO} ODCs might protect these cells, as was found for human ODCs *in vitro* (Rone et al., 2016). Interestingly, this counterintuitive detrimental role of IGF1R signaling might also explain observations in Alzheimer's disease (Cohen et al., 2009) and ischemic models (Endres et al., 2007). In both studies, reduced IGF-1 signaling improves survival of animals and decreases neuronal loss and brain infarct size, respectively.

In summary, the described protection against EAE in absence of IGF1R signaling by mature ODCs highlights the importance of this cell type in CNS homeostasis and in their dynamic interplay with the immune system. Our results also stress the complexity of IGF-1 mediated pathways and indicate a detrimental role of IGF1R signaling in mature ODCs during neuroinflammation.

4 | MATERIALS AND METHODS

4.1 | Mouse breeding and animal experimentation

Mice carrying a loxP-flanked *Igf1r* locus (*IGF1R^f*; *Igf1r*^{tm1jcbn}) (Klötting et al., 2008) were crossed to mice with the gene of the Cre

recombinase introduced into the *Mog* locus (*MOGi-cre*; *Mog*^{tm1[cre]Gkl}) (Hovelmeyer et al., 2005). Animals homozygous for the *IGF1R^f* allele and heterozygous for the *MOGi-cre* allele are denoted as *oIGF1R*^{-/-} mice. C57BL/6J mice for control groups were obtained from Janvier. *ROSA26YFP* (*B6.129X1-Gt(ROSA)26Sortm^{1(EYFP)Cos/J}*) (Srinivas et al., 2001) were obtained from Andreas Diefenbach and crossed to *MOGi-cre*, the heterozygous double mutants were denoted *oIGF1R*^{EYFP}. All animals were kept under SPF and barrier conditions according to Swiss and German animal law and institutional guidelines (permit numbers 101 [CH], 177 [CH], 07-12 [DE]). Presence of respective transgenes was confirmed by PCR analysis on DNA from tail biopsies by use of the following primer pairs: *MOGi-cre* (WT 350 bp) GAC AAT TCA GAG TGA TAG GAC CAG GGT ATC CC and GCT GCC TAT TAT TGG TAA GAG TGG; *MOGi-cre* (knock-in, 700 bp) TCC AAT TTA CTG ACC GTA CAC and CAT CAG CTA CAC CAG AGA CGG AAA TC; *IGF1R* TCC CTC AGG CTT CAT CCG CAA and CTT CAG CTT TGC AGG TGC ACG (WT, 300 bp; floxed, 350 bp); *EYFP* (200 bp) CTA TAT CAT GGC CGA CAA GC and ACT GGG TGC TCA GGT AGT GG. *In vivo* Cre-mediated recombination of *IGF1R* allele was confirmed by use of CCC AAA CAG ACC ACC ACC A and CTT CAG CTT TGC AGG TGC ACG (floxed, 1350 bp; recombined, 570 bp). Experiments were performed with both sexes. Animal experiments were performed with permits under Swiss and German law obtained from Swiss Cantonal and German regional authorities, respectively (Permit numbers 55.2-1-54-2532-1-12 ZH13/06, ZH002/15, ZH141/15, ZH195/18, ZH70/19), involving institutional animal welfare officers and Cantonal and regional animal experimentation commissions.

4.2 | Motor testing and disease models

In RotaRod experiments, the mice were placed on the drum in three consecutive trials with an acceleration from 5 to 50 rpm in 3 min and time to fall was recorded. For cuprizone intoxication, mice were fed for 5 weeks with 0.2% cuprizone (Sigma) mixed with ground food pellets and then returned to normal chow. For EAE experiments 6 to 10 weeks old mice were immunized subcutaneously with 200 μ g (each flank 100 μ g) of myelin oligodendrocyte glycoprotein MOG₃₅₋₅₅ peptide (M4939, Invitrogen) emulsified in Complete Freund's Adjuvant (CFA, H37 Ra, Difco laboratories), followed immediately and at day 2 by i.p. injection of 200 ng pertussis toxin (Sigma). The EAE score was calculated as follows: 0, no detectable signs of EAE; 0.5, distal limp tail; 1, complete limp tail; 1.5, limp tail and hind limb weakness; 2, unilateral partial hind limb paralysis; 2.5, bilateral partial hind limb paralysis; 3 complete bilateral hind limb paralysis; 3.5, complete hind limb paralysis and unilateral forelimb paralysis; 4, total paralysis of fore and hind limbs; 5, death.

4.3 | Flow cytometry and proliferation assay

Flow cytometric analysis of CNS-invading cells and proliferation assays were performed as described in Locatelli et al. (2012). For

staining of CNS cells, tissue was dissected and collected into 15 ml tubes containing 5 ml Sigma RPMI (Sigma) supplemented with 0.2 mg/ml Collagenase D (Roche Molecular Products) and 0.1 mg/ml DNase I. Tubes were placed on a water bath at 37°C, and the content was resuspended twice for 1 min with a 10 ml serological pipette (Sarstedt) and let to rest for 5 min. The suspension was filtered through a 70 µm cell strainer into a 50 ml collection tube and further mashed with the plunger of a syringe. Samples were centrifuged at 4°C for 10 min at 1500 rpm. The pellet was resuspended in 10 ml phosphate-buffered saline (PBS) and 11 ml were transferred to 15 ml collection tubes. The cell suspension was mixed with 30% Percoll (GE healthcare) and centrifuged in a swinging rotor centrifuge for 59 min at 5000 rpm at 4°C without brakes. The interphase containing the cells was collected and centrifuged for 10 min at 1200 rpm and 4°C. For intracellular staining, cells were incubated with 50 ng/mL PMA and 1 µg/ml Ionomycin for 4 h 30 min at 37°C, 5% CO₂, 90% humidity. Afterwards, the cells were centrifuged for 5 min at 1200 rpm and 4°C, and stained for surface markers and incubated for 30 min in the dark and at 4°C. For Foxp3 staining, cells were fixed for 1 h at room temperature, in the dark, with 200 µl of eBioscience™ Foxp3/ Transcription Factor Staining Buffer Set (according to manufacturer instructions).

The live/dead staining was purchased from Invitrogen. The following antibodies were purchased from BD Biosciences: XMG1.2 (IFN-γ), TC11-18H10 (IL17), 53-6.7 (CD8), N418 (CD11c), 7 AD/PC61 (CD25), IM7 (CD44), 30-F11 (CD45), M1/70 (CD11b) and M5/114 (MHC-II) antibodies from BD Biosciences, SA367H8 (CD95), NOK1 (CD95L), RM4-5 (CD4), MP1-22E9 (GM-CSF) antibodies from Biolegend, FJK-16 s (Foxp3) from eBioscience. Data was acquired with LSR II Fortessa (BD) and analyzed with Flow Jo version 10 (BD).

4.4 | Proliferation/thymidine incorporation assay

For radioactive proliferation assays, we activated 2×10^5 lymph node cells per well with 60 µg/ml of OVA (Research Genetics) or MOG₃₅₋₅₅ (Genscript) with or without 5 µg/ml antibody to CD28 (37 N, Bioexpress) in complete IMDM (Sigma-Aldrich) in a 96-well plate in quadruplicates, cultured at 5% CO₂.

4.5 | Microglia cultures

Cortex was removed from 1–3 days-old C57Bl/6 N pups, dissociated for 15 min in 1 mg/ml trypsin and 2 min in 1 mg/mL trypsin inhibitor. Cells were cultured in Dulbecco's modified Eagle (DMEM) consisting of Hams F12 (50/50, Sigma), supplemented with 10% Fetal calf serum (FCS), 100 U/ml penicillin, 100 µg/mL streptomycin and 2 mM glutamine. After 2 days of in vitro cultivation, the growth medium was completely replaced by fresh medium. After 10–14 days, flasks were mechanically shaken for 60 min, 150 r.p.m. to yield microglia in the supernatant, which were sub-cultured into uncoated 96 well plates (15,000 cells/well). They were kept in 70% astrocyte conditioned

medium and 30% fresh DMEM/F12 supplemented with 10% Fetal calf serum (FCS), 100 U/ml penicillin, 100 µg/ml streptomycin and 2 mM glutamine for 1–2 days to obtain steady-state microglia. For all experiments, primary microglial cells were used only after the first and second passage. After 24 h, the cells were treated with IGF-1 (500 ng/ml, Cadarlane) in the absence of serum in the medium. Afterwards, microglia were activated with recombinant mouse (rm)TNF-α (100 ng/ml (Peprotech) and rmIFN-γ 50 U/ml (Tebu-bio) or combined rmTNF-α and rmIFN-γ in the presence or absence of IGF-1 (500 ng/ml. MHCII and CD44 expression levels were determined by FACS analysis 24 h after onset of rmTNF-α and rmIFN-γ exposure in the presence and absence of IGF-1 pre-treatment (10,000 cells/sample).

4.6 | xCELLigence impedance-based system

xCELLigence system Real-Time Cell Analyzer RTCA-MP (Roche Diagnostics) allows tracking cell resistance or impedance, depicted as cell index values (CI) and normalization were performed using the RTCA Software 1.2 (Roche Diagnostics). The normalization of cell index (NCIti) arbitrarily sets the cell index values to 1 at the indicated time points. Primary microglial cells were seeded at a density of 15,000 cells/well in 96-well E-plate (Roche Diagnostics). Prior to plating, background impedance was determined and always subtracted as blank value. At short time after each treatment, the cell index drastically drops for 30–60 min due to the media change and temperature difference (Diemert et al., 2012), followed by a total recovery to values before media change or drug treatment.

4.7 | Histology

Mice were euthanized with CO₂ and perfused with PBS. For cryostat sections the tissue was fixed overnight with 4% paraformaldehyde (PFA), cryoprotected in 30% sucrose and frozen at –80°C. Frozen tissue was cut sagittally in 40 µm thick sections and stained as described before (Locatelli et al., 2012) with antibodies or antisera against following antigens: GFAP (DAKO, Q28115), aspartoacylase (ASPA; rabbit polyclonal serum, Dr. Matthias Klugmann, Mainz, Germany), proteolipid protein (PLP; rat, homemade), nerve glia antigen 2 (NG2; rat monoclonal, Dr. Jacqueline Trotter, Mainz, Germany), ionized calcium binding adaptor molecule 1 (Iba1; rabbit polyclonal, Wako Pure Chemical Industries), MHCII-specific antibody (rat, BD Biosciences), tomato lectin (FITC conjugated, L9386, Sigma-Aldrich), APC-specific antibody (CC1, Sigma-Aldrich), IGF1R-specific antibody (ab131476, Abcam). Detection was accomplished using either horseradish peroxidase-conjugated secondary antibodies or biotinylated secondary antibodies, streptavidin-horseradish peroxidase (Vector Laboratories) and 3,3' diaminobenzidine (DAB; Sigma-Aldrich). For immunofluorescent stainings, sections were covered with Vectashield (Vector Laboratories) and analyzed by confocal (Leica SP5/Zeiss LSM800) or fluorescence (Olympus BX50) microscope. For paraffin



sections, stainings for hematoxylin–eosin (H&E), Nissl as well as Luxol Fast Blue and Periodic Acid Schiff (LFB/PAS), ionized calcium binding adaptor molecule 1 (Iba1; rabbit, Wako), aspartoacylase (ASPA; rabbit polyclonal serum, Dr. Matthias Klugmann, Mainz, Germany) were performed as indicated in Locatelli et al. (2012). For NF staining, paraffin sections were first dewaxed and rehydrated followed by antigen retrieval in citrate buffer pH 6.0 for 10 min. Sections were then incubated in 0.3% of hydrogen peroxide and blocked with 3% normal goat serum (NGS) and 0.3% Triton X100 in PBS. NF-specific antibody (N4142, Millipore) was incubated for 12 h at room temperature. A biotinylated secondary antibody (goat anti-mouse, Vector) was used for detection. The staining with DAB was developed using Vectastain ABC kit (Vector) according to the manufacturer's protocols. Sections were counterstained for 2 min with hemalaun (Dr. Hollborn and Sons).

4.8 | Immunoblotting

Mouse tissue was digested in lysis buffer (Tris-Cl 35 mM, NaCl 150 mM, NP-40 1%, Sodium deoxycholate 0.5%, Triton 1%, Na₃VO₄ 1 mM, leupatin 1 µg/ml, NaF 5 mM, PMSF 5 mM) for 30', sonicated and centrifuged at 13,000 rpm at 4°C for 20 min. Protein concentration was quantified with a BCA assay (Thermo Scientific). Proteins were detected with anti-Vinculin (Cell Signaling), anti-MOG (818C5, homemade), anti-MBP (Santa-Cruz), anti-NG2 (Millipore). Samples for anti-NG2 immunoblotting were previously digested with Chondroitinase ABC (Seikagaku) for 1 h at 37°C.

4.9 | RNA isolation

Samples were homogenized in 1 ml TRIZOL (Sigma-Aldrich) and incubated for 5 min at room temperature (RT). 200 µl chloroform per sample were added, incubated for 3 min at RT, and centrifuged at 8000 rpm for 15 min at 4°C. The aqueous phase containing RNA was transferred into a fresh tube and precipitated adding 500 µl isopropyl alcohol after 10 min incubation at RT and centrifugation at 800 rpm for 10 min at 4°C. The supernatant was removed, and the RNA pellet washed with 1 ml 75% ethanol. Samples were centrifuged at 5000 rpm for 5 min at 4°C and the RNA pellet then was let drying out for 15 min at RT. The RNA was finally dissolved in 45 µl RNase free water with 5 µl of 10x incubation buffer and 1 µl DNaseI. The samples were incubated at 37°C for 20 min, then 1 µl 0.5 M EDTA was added and incubated at 75°C for 10 min and finally chilled on ice.

4.10 | cDNA synthesis

1 µl random primers (100 ng/µl), 1 µl dNTP (10 mM), 4 µl First-strand buffer (5x), 2 µl DTT (0.1 M), and 1 µl RNase OUT were incubated for 2 min at 37°C and then 1 µl M-MLV RT (200 U/µl) was added. 5 µg RNA was diluted in 10 µl RNase free H₂O, heated to 65°C for 5 min

and quenched on ice. Afterwards, 10 µl Master Mix were added to the RNA, incubated 10 min at 21°C, 50 min at 37°C and finally 15 min at 70°C. The cDNA was finally diluted 1:10.

4.11 | RNA array

oIGF1R^{-/-} and control female animals were induced with EAE and sacrificed after 9 days. RNA was isolated from spinal cord tissue and assessed by microarray analysis ($n = 5$). Total RNA was labeled and hybridized to Affymetrix GeneChip[®] Mouse Gene 1.0 ST arrays according to the manufacturer's instructions. We used the oligo package to import and process the scanned arrays into R (Carvalho & Irizarry, 2010). Further, we assessed the quality of scanned arrays with array Quality Metrics (Kauffmann et al., 2009). "Robust multichip average" was then used for background correction, normalization and to control for technical variation between arrays within the study (Irizarry et al., 2003). For annotation, we used both the original Affymetrix probe set and an updated probe grouping provided by Brainarray (Dai et al., 2005). Only probe sets that map to a unique gene were considered for further analysis. Then, a linear model was fitted to each of the remaining probe set's expression data, and the estimated coefficients given the set of contrasts were computed using Limma (Smyth, 2004). Due to high variability in disease progression and small sample size, the list of differentially expressed genes was reported without adjusting for multiple testing and should be interpreted with caution.

4.12 | Electron microscopy

Electron microscopy analyses were performed as previously described (Locatelli et al., 2012). Briefly, animals were sacrificed and transcardially perfused with saline followed by a fixative containing 4% paraformaldehyde (Serva, Heidelberg, Germany) and 2% glutaraldehyde (Serva) in PBS. After post-fixation for 24 hours in the same fixative, the tissue was rinsed and cut into sections of 50 to 60 µm using a vibrating microtome (Leica Microsystems, Wetzlar, Germany). The sections were stained with 0.5% osmium tetroxide (EMS, Hatfield, PA, USA). After rinsing in PBS, the sections were dehydrated in graded alcohol and further stained with 1% uranyl acetate (Merck, Darmstadt, Germany) in 70% alcohol. After final dehydration the sections were transferred in propylene oxide (Sigma Aldrich, Steinheim, Germany) and incubated in Durcupan (Sigma Aldrich) between coated microscope slides and cover glasses. After polymerization at 56°C for 48 h, the cover glasses were removed and the sections were mounted on blocks of resin, followed by final polymerization. Areas of interest were trimmed and cut using an ultra-microtome (Leica Microsystems). Ultra-thin sections with an average thickness of 55 nm were transferred on formvar-coated copper grids and stained with lead citrate. Analysis was performed using a Zeiss SIGMA electron microscope (Zeiss NTS, Oberkochen, Germany) equipped with a STEM detector and ATLAS software. Morphology and ultra-structure of myelin sheaths and ODCs was evaluated in the corpus callosum and cerebellar fiber tracts.

4.13 | Single-cell RNA sequencing data preprocessing

Human MS single-nucleus RNA-Sequencing data and the corresponding metadata were downloaded from Gene Expression Omnibus accession number GSE118257 and normalized using the R package RaceID version 0.2.3 run under R version 4.0.2. RaceID was run using default parameters with the following adjustments. Cells with minimal transcript counts above the 25th percentile, that is, 747 genes, were included. The CCcorrect function was run using dimensional reduction ($\text{dimR} = \text{TRUE}$) on 20 principal components ($\text{nComp} = 20$), the following batch effect associated genes were excluded using the CGenes function: JUN, FOS, ZFP36, HISPA1A, HISPA1B, DUST1, EGR1, and MALAT1. Clustering was run with the cln parameter of the clustexp function set to 22.

4.14 | Single-cell RNA sequencing data visualization

Data processing was conducted using the Tidyverse R package version 1.3.1. Gene expression data was visualized using the ggplot2 R package version 3.3.3. Normalized gene expression of IGFR1 was plotted across cell types and disease stages. For improved readability, clusters with less than 1% of all cells (i.e., <133 cells) and data from underrepresented cell types (Macrophages with 13 cells, and vascular smooth muscle cells with 1 cell) were excluded from the final plot.

4.15 | Code availability

The code to reproduce the single-cell RNA-Sequencing figure can be found under: https://github.com/rsankowski/locatelli_ms_celltype_comparison.

4.16 | Statistics

Statistical analysis was performed using GraphPad Prism 8 (La Jolla, CA, USA). All values are presented as mean \pm SEM. Asterisks indicate significant differences ($*p < .05$, $**p < .01$, and $***p < .001$, $****p < .0001$). Animals were allocated randomly and experiments performed blindly where necessary (see also figure legends). Following validation of normal distribution, unpaired t -test was used for the analysis in Figure 1e, Figure 2b,e,g, Figure 3a,b,d,f, Figure 4d-h, Supplementary Figure 1c,d, Supplementary Figure 2a,c. When not normally distributed, data was compared using the Mann Whitney U test in Figures 4b and 5a-f. One-way ANOVA with Bonferroni post-hoc analysis was used in Supplementary Figure 4a,c,d and Supplementary Figure 5b. In Figure 5h and Supplementary Figure 6b,c, results are given as mean values \pm S.D. and tested with 1 way ANOVA and Scheffé's multiple comparison test.

AUTHOR CONTRIBUTIONS

Thorsten Buch and Burkhard Becher conceived the experimental system. Giuseppe Locatelli, Filipa Marques-Ferreira, Martin Krueger, Barbara Ingold-Heppner, Olivia Prazeres da Costa, Amalia Dolga, Magdalena Huber, Maike Gold, Sabrina Walthert, Vladislava Milchevska, Roman Sankowski, Antonis Katsoulas, and Vasileia Kalaitzaki carried out the experiments and analyzed the data. Thorsten Buch, Ari Waisman, Ingo Bechmann, Carsten Culmsee, Achim Tresch, Marco Prinz, and Burkhard Becher supervised the work. Giuseppe Locatelli and Thorsten Buch wrote the manuscript.

ACKNOWLEDGMENTS

We are grateful for support by the technician and mouse teams in Zurich, Cologne, Bern, and Munich. We thank Andreas Diefenbach for providing *ROSA26YFP* mice and Jens Brüning for providing the *IGF1R floxed* model. We thank the flow cytometry facilities of the University of Zurich and the medical faculty of the Technische Universität München for their support. We thank Daniela Ivan for support in histological preparations. We thank Martin Stangel, Dirk Busch, Bettina Schreiner, and Iana Parvanova for their help in manuscript preparation. We especially thank Jon Laman for extensive help in manuscript editing. We are grateful for the support by the Swiss Staatssekretariat für Bildung und Forschung SBF (COST action BM0603 NEURINFNET to Thorsten Buch and Burkhard Becher), the Swiss National Foundation (SNF 310030_197652/1 to Thorsten Buch), the German Research Foundation DFG (TR22 to Thorsten Buch), the Swiss Multiple Sclerosis Society (Thorsten Buch and Giuseppe Locatelli, grant no. 2021-02 and 2021-07), the Hertie Foundation (P1150013 to Thorsten Buch), the Bonnizzi-Theler Foundation (Thorsten Buch) and Scherbarth Foundation (Giuseppe Locatelli). Antonis Katsoulas and Vasileia Kalaitzaki were supported by the ARSEP foundation. Marco Prinz was supported by the Sobek Foundation, the Ernst Jung Foundation, the Novo Nordisk Prize, the DFG SFB992 (Project ID 192904750), SFB1160 (Project ID 256073931), CRC/TRR167 "NeuroMac," Project ID 259373024, the DFG under Germany's Excellence Strategy (CIBSS-EXC-2189-Project ID 390939984), Reinhart-Koselleck-Grant (Project ID 279642606) and Gottfried Wilhelm Leibniz Prize, the Alzheimer Forschung Initiative e.V. (AFI) and the Ministry of Science, Research and Arts, Baden-Wuerttemberg (Sonderlinie "Neuroinflammation"). Marco Prinz and Roman Sankowski were supported by the DFG CRC1479 (Project ID 441891347). Roman Sankowski was supported by the Else Kröner Fresenius Foundation. Open Access funding enabled and organized by Projekt DEAL.

CONFLICT OF INTEREST

The authors declare no competing interests.

DATA AVAILABILITY STATEMENT

The data that support the findings of this study are available from the corresponding author upon reasonable request.

ORCID

Giuseppe Locatelli  <https://orcid.org/0000-0002-2179-4407>

Antonis Katsoulas  <https://orcid.org/0000-0001-8138-7646>



Vasileia Kalaitzaki <https://orcid.org/0000-0002-4158-2321>

Roman Sankowski <https://orcid.org/0000-0001-9215-8021>

Magdalena Huber <https://orcid.org/0000-0002-2963-0693>

Carsten Culmsee <https://orcid.org/0000-0002-5121-5015>

Ari Waisman <https://orcid.org/0000-0003-4304-8234>

Ingo Bechmann <https://orcid.org/0000-0002-6805-1555>

Vladislava Milchevskaya <https://orcid.org/0000-0002-4350-8424>

Marco Prinz <https://orcid.org/0000-0002-0349-1955>

Achim Tresch <https://orcid.org/0000-0002-4146-6371>

Burkhard Becher <https://orcid.org/0000-0002-1541-7867>

Thorsten Buch <https://orcid.org/0000-0002-2236-9074>

REFERENCES

- Adams, T. E., Epa, V. C., Garrett, T. P., & Ward, C. W. (2000). Structure and function of the type 1 insulin-like growth factor receptor. *Cellular and Molecular Life Sciences*, 57(7), 1050–1093.
- Anlar, B., Sullivan, K. A., & Feldman, E. L. (1999). Insulin-like growth factor-I and central nervous system development. *Hormones et Métabolisme*, 31(2–3), 120–125.
- Arpa, J., Sanz-Gallego, I., Medina-Báez, J., Portela, L. V. C., Jardim, L. B., Torres-Aleman, I., & Saute, J. A. M. (2011). Subcutaneous insulin-like growth factor-1 treatment in spinocerebellar ataxias: An open label clinical trial. *Movement Disorders*, 26(2), 358–359.
- Beck, K. D., Powell-Braxton, L., Widmer, H. R., Valverde, J., & Hefti, F. (1995). Igf1 gene disruption results in reduced brain size, CNS hypomyelination, and loss of hippocampal granule and striatal parvalbumin-containing neurons. *Neuron*, 14(4), 717–730.
- Benarroch, E. E. (2009). Oligodendrocytes: Susceptibility to injury and involvement in neurologic disease. *Neurology*, 72(20), 1779–1785.
- Benetti, F., Ventura, M., Salmini, B., Ceola, S., Carbonera, D., Mammi, S., Zitolo, A., D'Angelo, P., Urso, E., & Maffia, M. (2010). Cuprizone neurotoxicity, copper deficiency and neurodegeneration. *Neurotoxicology*, 31(5), 509–517.
- Bilbao, D., Luciani, L., Johannesson, B., Piszczek, A., & Rosenthal, N. (2014). Insulin-like growth factor-1 stimulates regulatory T cells and suppresses autoimmune disease. *EMBO Molecular Medicine*, 6(11), 1423–1435.
- Cannella, B., Pitt, D., Capello, E., & Raine, C. S. (2000). Insulin-like growth factor-1 fails to enhance central nervous system myelin repair during autoimmune demyelination. *The American Journal of Pathology*, 157(3), 933–943.
- Carro, E., Trejo, J. L., Gomez-Isla, T., LeRoith, D., & Torres-Aleman, I. (2002). Serum insulin-like growth factor I regulates brain amyloid-beta levels. *Nature Medicine*, 8(12), 1390–1397.
- Carson, M. J., Behringer, R. R., Brinster, R. L., & McMorris, F. A. (1993). Insulin-like growth factor I increases brain growth and central nervous system myelination in transgenic mice. *Neuron*, 10(4), 729–740.
- Carvalho, B. S., & Irizarry, R. A. (2010). A framework for oligonucleotide microarray preprocessing. *Bioinformatics*, 26(19), 2363–2367. <https://doi.org/10.1093/bioinformatics/btq431>
- Cheng, C. M., Joncas, G., Reinhardt, R. R., Farrer, R., Quarles, R., Janssen, J., McDonald, M. P., Crawley, J. N., Powell-Braxton, L., & Bondy, C. A. (1998). Biochemical and morphometric analyses show that myelination in the insulin-like growth factor 1 null brain is proportionate to its neuronal composition. *The Journal of Neuroscience*, 18(15), 5673–5681.
- Chesik, D., De Keyser, J., & Wilczak, N. (2008). Insulin-like growth factor system regulates oligodendroglial cell behavior: Therapeutic potential in CNS. *Journal of Molecular Neuroscience*, 35(1), 81–90.
- Cohen, E., Paulsson, J. F., Blinder, P., Burstyn-Cohen, T., Du, D., Estepa, G., Adame, A., Pham, H. M., Holzenberger, M., Kelly, J. W., Masliah, E., & Dillin, A. (2009). Reduced IGF-1 signaling delays age-associated proteotoxicity in mice. *Cell*, 139(6), 1157–1169. <https://doi.org/10.1016/j.cell.2009.11.014>
- Cuscik, M. F., Libbey, J. E., Trede, N. S., & Fujinami, R. S. (2014). Targeting insulin-like growth factor 1 leads to amelioration of inflammatory demyelinating disease. *PLoS One*, 9(4), e94486.
- Dai, M., Wang, P., Boyd, A. D., Kostov, G., Athey, B., Jones, E. G., Bunney, W. E., Myers, R. M., Speed, T. P., Akil, H., Watson, S. J., & Meng, F. (2005). Evolving gene/transcript definitions significantly alter the interpretation of GeneChip data. *Nucleic Acids Research*, 33(20), e175. <https://doi.org/10.1093/nar/gni179>
- D'Ercole, A. J., Ye, P., & O'Kusky, J. R. (2002). Mutant mouse models of insulin-like growth factor actions in the central nervous system. *Neuropeptides*, 36(2–3), 209–220.
- Diemert, S., Dolga, A. M., Tobaben, S., Grohm, J., Pfeifer, S., Oexler, E., & Culmsee, C. (2012). Impedance measurement for real time detection of neuronal cell death. *Journal of Neuroscience Methods*, 203, 69–77.
- DiToro, D., Harbour, S. N., Bando, J. K., Benavides, G., Witte, S., Laufer, V. A., Moseley, C., Singer, J. R., Frey, B., Turner, H., Bruning, J., Darley-Usmar, V., Gao, M., Conover, C., Hatton, R. D., Frank, S., Colonna, M., & Weaver, C. T. (2020). Insulin-like growth factors are key regulators of T helper 17 regulatory T cell balance in autoimmunity. *Immunity*, 52(4), 650–667.e10. <https://doi.org/10.1016/j.immuni.2020.03.013>
- Dolga, A. M., Letsche, T., Gold, M., Doti, N., Bacher, M., Chiamvimonvat, N., Dodel, R., & Culmsee, C. (2012). Activation of KCNN3/SK3/K(Ca)2.3 channels attenuates enhanced calcium influx and inflammatory cytokine production in activated microglia. *Glia*, 60(12), 2050–2064.
- Endres, M., Piriz, J., Gertz, K., Harms, C., Meisel, A., Kronenberg, G., & Torres-Aleman, I. (2007). Serum insulin-like growth factor I and ischemic brain injury. *Brain Research*, 1185, 328–335. <https://doi.org/10.1016/j.brainres.2007.09.053>
- Fernandez, A. M., & Torres-Aleman, I. (2012). The many faces of insulin-like peptide signaling in the brain. *Nature Reviews Neuroscience*, 13(4), 225–239.
- Floyd, S. C., Favre, C., Lasorsa, F. M., Leahy, M., Trigiant, G., Stroebel, P., Marx, A., Loughran, G., O'Callaghan, K., Marobbio, C. M., Slotboom, D. J., Kunji, E. R., Palmieri, F., & O'Connor, R. (2007). The insulin-like growth factor-I-mTOR signaling pathway induces the mitochondrial pyrimidine nucleotide carrier to promote cell growth. *Molecular Biology of the Cell*, 18(9), 3545–3555.
- Frank, J. A., Richert, N., Lewis, B., Bash, C., Howard, T., Civil, R., Stone, R., Eaton, J., McFarland, H., & Leist, T. (2002). A pilot study of recombinant insulin-like growth factor-1 in seven multiple sclerosis patients. *Multiple Sclerosis*, 8(1), 24–29.
- French, H. M., Reid, M., Mamontov, P., Simmons, R. A., & Grinspan, J. B. (2009). Oxidative stress disrupts oligodendrocyte maturation. *Journal of Neuroscience Research*, 87(14), 3076–3087.
- Funfschilling, U., et al. (2012). Glycolytic oligodendrocytes maintain myelin and long-term axonal integrity. *Nature*, 485(7399), 517–521.
- Genoud, S., Maricic, I., Kumar, V., & Gage, F. H. (2005). Targeted expression of IGF-1 in the central nervous system fails to protect mice from experimental autoimmune encephalomyelitis. *Journal of Neuroimmunology*, 168(1–2), 40–45.
- Hovelmeyer, N., Hao, Z., et al. (2005). Apoptosis of oligodendrocytes via Fas and TNF-R1 is a key event in the induction of experimental autoimmune encephalomyelitis. *Journal of Immunology*, 175(9), 5875–5884.
- Huyhn, J. L., et al. (2014). Epigenome-wide differences in pathology-free regions of multiple sclerosis-affected brains. *Nature Neuroscience*, 17(1), 121–130.
- Ip, C. W., Kroner, A., Bendszus, M., Leder, C., Kobsar, I., Fischer, S., Wiendl, H., Nave, K. A., & Martini, R. (2006). Immune cells contribute to myelin degeneration and axonopathic changes in mice overexpressing proteolipid protein in oligodendrocytes. *The Journal of Neuroscience*, 26(31), 8206–8216.

- Irizarry, R. A., Hobbs, B., Collin, F., et al. (2003). Exploration, normalization, and summaries of high density oligonucleotide array probe level data. *Biostatistics*, 4(2), 249–264.
- Jäkel, S., Agirre, E., Mendanha Falcão, A., van Bruggen, D., Lee, K. W., Knuesel, I., Malhotra, D., Ffrench-Constant, C., Williams, A., & Castelo-Branco, G. (2019). Altered human oligodendrocyte heterogeneity in multiple sclerosis. *Nature*, 566(7745), 543–547. <https://doi.org/10.1038/s41586-019-0903-2>
- Kassmann, C. M., Lappe-Siefke, C., Baes, M., Brügger, B., Mildner, A., Werner, H. B., Natt, O., Michaelis, T., Prinz, M., Frahm, J., & Nave, K. A. (2007). Axonal loss and neuroinflammation caused by peroxisome-deficient oligodendrocytes. *Nature Genetics*, 39(8), 969–976.
- Kauffmann, A., Gentleman, R., & Huber, W. (2009). ArrayQualityMetrics—a bioconductor package for quality assessment of microarray data. *Bioinformatics*, 25(3), 415–416.
- Kerschensteiner, M., Meinel, E., & Hohlfeld, R. (2009). Neuro-immune crosstalk in CNS diseases. *Neuroscience*, 158(3), 1122–1132.
- Khwaja, O., & Volpe, J. J. (2008). Pathogenesis of cerebral white matter injury of prematurity. *Archives of Disease in Childhood. Fetal and Neonatal Edition*, 93(2), 153–161.
- Klötting, N., et al. (2008). Autocrine IGF-1 action in adipocytes controls systemic IGF-1 concentration and growth. *Diabetes*, 57(8), 2074–2082.
- Koutouros, M., Berer, K., Kawakami, N., Wekerle, H., & Krishnamoorthy, G. (2014). Treg cells mediate recovery from EAE by controlling effector T cell proliferation and motility in the CNS. *Acta Neuropathologica Communications*, 2, 163.
- Labandeira-Garcia, J. L., Costa-Besada, M. A., Labandeira, C. M., Villar-Cheda, B., & Rodríguez-Perez, A. I. (2017). Insulin-like growth factor-1 and neuroinflammation. *Frontiers in Aging Neuroscience*, 9, 365.
- Lanzillo, R., di Somma, C., Quarantelli, M., Ventrella, G., Gasperi, M., Prinster, A., Vacca, G., Pivonello, C., Orefice, G., Colao, A., & Morra, V. B. (2011). Insulin-like growth factor (IGF)-I and IGF-binding protein-3 serum levels in relapsing-remitting and secondary progressive multiple sclerosis patients. *European Journal of Neurology*, 18(12), 1402–1406.
- Lee, Y., Morrison, B. M., Li, Y., Lengacher, S., Farah, M. H., Hoffman, P. N., Liu, Y., Tsingalia, A., Jin, L., Zhang, P. W., Pellerin, L., Magistretti, P. J., & Rothstein, J. D. (2012). Oligodendroglia metabolically support axons and contribute to neurodegeneration. *Nature*, 487(7408), 443–448.
- Li, W., Quigley, L., Yao, D. L., Hudson, L. D., Brenner, M., Zhang, B. J., Brocke, S., McFarland, H., & Webster, H. D. (1998). Chronic relapsing experimental autoimmune encephalomyelitis: Effects of insulin-like growth factor-I treatment on clinical deficits, lesion severity, glial responses, and blood brain barrier defects. *Journal of Neuropathology and Experimental Neurology*, 57(5), 426–438.
- Lin, W., et al. (2007). The integrated stress response prevents demyelination by protecting oligodendrocytes against immune-mediated damage. *The Journal of Clinical Investigation*, 117, 448–456.
- Liu, X., Yao, D. L., & Webster, H. (1995). Insulin-like growth factor I treatment reduces clinical deficits and lesion severity in acute demyelinating experimental autoimmune encephalomyelitis. *Multiple Sclerosis*, 1(1), 2–9.
- Locatelli, G., Baggiolini, A., Schreiner, B., Palle, P., Waisman, A., Becher, B., & Buch, T. (2015). Mature oligodendrocytes actively increase in vivo cytoskeletal plasticity following CNS damage. *Journal of Neuroinflammation*, 2(12), 62.
- Locatelli, G., Wörtge, S., Buch, T., Ingold, B., Frommer, F., Sobottka, B., Krüger, M., Karram, K., Bühlmann, C., Bechmann, I., Heppner, F. L., Waisman, A., & Becher, B. (2012). Primary oligodendrocyte death does not elicit anti-CNS immunity. *Nature Neuroscience*, 15(4), 543–550.
- Lovett-Racke, A. E., Bittner, P., Cross, A. H., Carlino, J. A., & Racke, M. K. (1998). Regulation of experimental autoimmune encephalomyelitis with insulin-like growth factor (IGF-1) and IGF-1/IGF-binding protein-3 complex (IGF-1/IGFBP3). *The Journal of Clinical Investigation*, 101(8), 1797–1804.
- Lucchinetti, C., Bruck, W., Parisi, J., Scheithauer, B., Rodriguez, M., & Lassmann, H. (1999). A quantitative analysis of oligodendrocytes in multiple sclerosis lesions. A study of 113 cases. *Brain*, 122(Pt 12), 2279–2295.
- Mason, J. L., Xuan, S., Dragatsis, I., Efstratiadis, A., & Goldman, J. E. (2003). Insulin-like growth factor (IGF) signaling through type 1 IGF receptor plays an important role in remyelination. *The Journal of Neuroscience*, 23(20), 7710–7718.
- Mason, J. L., Ye, P., Suzuki, K., D'Ercole, A. J., & Matsushima, G. K. (2000). Insulin-like growth factor-1 inhibits mature oligodendrocyte apoptosis during primary demyelination. *The Journal of Neuroscience*, 20(15), 5703–5708.
- Mastroeni, R., Bensadoun, J. C., Charvin, D., Aebischer, P., Pujol, A., & Raoul, C. (2009). Insulin-like growth factor-1 and neurotrophin-3 gene therapy prevents motor decline in an X-linked adrenoleukodystrophy mouse model. *Annals of Neurology*, 66(1), 117–122.
- McTigue, D. M., & Tripathi, R. B. (2008). The life, death, and replacement of oligodendrocytes in the adult CNS. *Journal of Neurochemistry*, 107(1), 1–19.
- Michalski, J.-P., Anderson, C., Beauvais, A., De Repentigny, Y., & Kothary, R. (2011). The proteolipid protein promoter drives expression outside of the oligodendrocyte lineage during embryonic and early postnatal development. *PLoS One*, 6(5), e19772. <https://doi.org/10.1371/journal.pone.0019772>
- Moore, S., Meschkat, M., Ruhwedel, T., Trevisiol, A., Tzvetanova, I. D., Battefeld, A., Kusch, K., Kole, M. H. P., Strenzke, N., Möbius, W., De Hoz, L., & Nave, K. A. (2020). A role of oligodendrocytes in information processing. *Nature Communications*, 11(1), 5497. <https://doi.org/10.1038/s41467-020-19152-7>
- Nagano, I., Ilijeva, H., Shiote, M., Murakami, T., Yokoyama, M., Shoji, M., & Abe, K. (2005). Therapeutic benefit of intrathecal injection of insulin-like growth factor-1 in a mouse model of amyotrophic lateral sclerosis. *Journal of the Neurological Sciences*, 235(1–2), 61–68.
- O'Donnell, S. L., Frederick, T. J., Krady, J. K., Vannucci, S. J., & Wood, T. L. (2002). IGF-I and microglia/macrophage proliferation in the ischemic mouse brain. *Glia*, 39(1), 85–97.
- Pang, Y., Zheng, B., Fan, L. W., Rhodes, P. G., & Cai, Z. (2007). IGF-1 protects oligodendrocyte progenitors against TNF α -induced damage by activation of PI3K/Akt and interruption of the mitochondrial apoptotic pathway. *Glia*, 55(11), 1099–1107.
- Pini, G., et al. (2012). IGF1 as a potential treatment for Rett syndrome: Safety assessment in six Rett patients. *Autism Research and Treatment*, 2012, 679801.
- Rone, M. B., Cui, Q. L., Fang, J., Wang, L. C., Zhang, J., Khan, D., Bedard, M., Almazan, G., Ludwin, S. K., Jones, R., Kennedy, T. E., & Antel, J. P. (2016). Oligodendroglial pathology in multiple sclerosis: Low glycolytic metabolic rate promotes oligodendrocyte survival. *Journal of Neuroscience*, 36(17), 4698–4707.
- Sevigny, J. J., Ryan, J. M., Van Dyck, C. H., Peng, Y., Lines, C. R., Nessly, M. L., & MK-677 Protocol 30 Study Group. (2008). Growth hormone secretagogue MK-677: No clinical effect on AD progression in a randomized trial. *Neurology*, 71(21), 1702–1708.
- Shahbazi, M., Abdolmohammadi, R., Ebadi, H., & Farazmandfar, T. (2017). Novel functional polymorphism in IGF-1 gene associated with multiple sclerosis: A new insight to MS. *Multiple Sclerosis and Related Disorders*, 13, 33–37.
- Smyth, G. K. (2004). Linear models and empirical bayes methods for assessing differential expression in microarray experiments. *Statistical Applications in Genetics and Molecular Biology*, 3, Article3–Article25.



- Solly, S. K., Thomas, J. L., Monge, M., Demerens, C., Lubetzki, C., Gardinier, M. V., Matthieu, J. M., & Zalc, B. (1996). Myelin/oligodendrocyte glycoprotein (MOG) expression is associated with myelin deposition. *Glia*, *18*(1), 39–48.
- Srinivas, S., Watanabe, T., Lin, C. S., William, C. M., Tanabe, Y., Jessell, T. M., & Costantini, F. (2001). Cre reporter strains produced by targeted insertion of EYFP and ECFP into the ROSA26 locus. *BMC Developmental Biology*, *1*(1), 4.
- Tropea, D., Giacometti, E., Wilson, N. R., Beard, C., McCurry, C., Fu, D. D., Flannery, R., Jaenisch, R., & Sur, M. (2009). Partial reversal of Rett syndrome-like symptoms in MeCP2 mutant mice. *PNAS*, *106*(6), 2029–2034.
- Vincent, A. M., Mobley, B. C., Hiller, A., & Feldman, E. L. (2004). IGF-I prevents glutamate-induced motor neuron programmed cell death. *Neurobiology of Disease*, *16*(2), 407–416.
- Werner, S. R., Saha, J. K., Broderick, C. L., Zhen, E. Y., Higgs, R. E., Duffin, K. L., & Smith, R. C. (2010). Proteomic analysis of demyelinated and remyelinating brain tissue following dietary cuprizone administration. *Journal of Molecular Neuroscience*, *42*(2), 210–225.
- Wilczak, N., Chesik, D., Hoekstra, D., & De Keyser, J. (2008). IGF binding protein alterations on periplaque oligodendrocytes in multiple sclerosis: Implications for remyelination. *Neurochemistry International*, *52*(8), 1431–1435.
- Wrigley, S., Arafa, D., & Tropea, D. (2017). Insulin-like growth factor 1: At the crossroads of brain development and aging. *Frontiers in Cellular Neuroscience*, *11*, 14.
- Yao, D. L., Liu, X., Hudson, L. D., & Webster, H. D. (1995). Insulin-like growth factor I treatment reduces demyelination and up-regulates gene expression of myelin-related proteins in experimental autoimmune encephalomyelitis. *PNAS*, *92*(13), 6190–6194.
- Ye, P., Li, L., Richards, R. G., DiAugustine, R. P., & D'Ercole, A. J. (2002). Myelination is altered in insulin-like growth factor-I null mutant mice. *The Journal of Neuroscience*, *22*(14), 6041–6051.
- Zatta, P., Raso, M., Zambenedetti, P., Wittkowski, W., Messori, L., Piccioli, F., Mauri, P. L., & Beltramini, M. (2005). Copper and zinc dismetabolism in the mouse brain upon chronic cuprizone treatment. *Cellular and Molecular Life Sciences*, *62*(13), 1502–1513.
- Zeger, M., Popken, G., Zhang, J., Xuan, S., Lu, Q. R., Schwab, M. H., Nave, K. A., Rowitch, D., D'Ercole, A. J., & Ye, P. (2007). Insulin-like growth factor type 1 receptor signaling in the cells of oligodendrocyte lineage is required for normal in vivo oligodendrocyte development and myelination. *Glia*, *55*(4), 400–411.
- Zeis, T., & Schaeren-Wiemers, N. (2008). Lame ducks or fierce creatures? The role of oligodendrocytes in multiple sclerosis. *Journal of Molecular Neuroscience: MN*, *35*(1), 91–100.

SUPPORTING INFORMATION

Additional supporting information can be found online in the Supporting Information section at the end of this article.

How to cite this article: Locatelli, G., Marques-Ferreira, F., Katsoulas, A., Kalaitzaki, V., Krueger, M., Ingold-Heppner, B., Walthert, S., Sankowski, R., Prazeres da Costa, O., Dolga, A., Huber, M., Gold, M., Culmsee, C., Waisman, A., Bechmann, I., Milchevskaya, V., Prinz, M., Tresch, A., Becher, B., & Buch, T. (2023). IGF1R expression by adult oligodendrocytes is not required in the steady-state but supports neuroinflammation. *Glia*, *71*(3), 616–632. <https://doi.org/10.1002/glia.24299>